

PAPER

Current correlations, Drude weights and large deviations in a box–ball system

To cite this article: Atsuo Kuniba *et al* 2022 *J. Phys. A: Math. Theor.* **55** 244006

View the [article online](#) for updates and enhancements.

You may also like

- [More current with less particles due to power-law hopping](#)
Madhumita Saha, Archak Purkayastha and Santanu K Maiti
- [Hubbard-to-Heisenberg crossover \(and efficient computation\) of Drude weights at low temperatures](#)
C Karrasch
- [Correlation functions and transport coefficients in generalised hydrodynamics](#)
Jacopo De Nardis, Benjamin Doyon, Marko Medenjak *et al.*



IOP | ebooks™

Bringing together innovative digital publishing with leading authors from the global scientific community.

Start exploring the collection—download the first chapter of every title for free.

Current correlations, Drude weights and large deviations in a box–ball system

Atsuo Kuniba¹ , Grégoire Misguich^{2,*}  and Vincent Pasquier² 

¹ Institute of Physics, University of Tokyo, Komaba, Tokyo 153-8902, Japan

² Université Paris-Saclay, CNRS, CEA, Institut de physique théorique, 91191 Gif-sur-Yvette, France

E-mail: atsuo.s.kuniba@gmail.com, gregoire.misguich@cea.fr and vincent.pasquier@ipht.fr

Received 31 January 2022, revised 3 April 2022

Accepted for publication 6 May 2022

Published 26 May 2022



Abstract

We explore several aspects of the current fluctuations and correlations in the box–ball system, an integrable cellular automaton in one space dimension. The state we consider is an ensemble of microscopic configurations where the box occupancies are independent random variables (i.i.d. state), with a given mean ball density. We compute several quantities exactly in such homogeneous stationary state: the mean value and the variance of the number of balls N_t crossing the origin during time t , and the scaled cumulants generating function associated to N_t . We also compute two spatially integrated current–current correlations. The first one, involving the long-time limit of the current–current correlations, is the so-called Drude weight and is obtained with thermodynamic Bethe ansatz (TBA). The second one, involving equal time current–current correlations is calculated using a transfer matrix approach. A family of generalized currents, associated to the conserved charges and to the different time evolutions of the models are constructed. The long-time limits of their correlations generalize the Drude weight and the second cumulant of N_t and are found to obey nontrivial symmetry relations. They are computed using TBA and the results are found to be in good agreement with microscopic simulations of the model. TBA is also used to compute explicitly the whole family of flux Jacobian matrices. Finally, some of these results are extended to a (non-i.i.d.) two-temperatures generalized Gibbs state (with one parameter coupled to the total number of balls, and another one coupled to the total number of solitons).

*Author to whom any correspondence should be addressed.

Keywords: box–ball system, Drude weight, integrability, generalized hydrodynamics, thermodynamic Bethe ansatz, large deviation

(Some figures may appear in colour only in the online journal)

1. Introduction

The box ball system (BBS) is an integrable cellular automaton introduced in 1990 by Takahashi and Satsuma [1]. In this model some ‘balls’ occupy the sites (‘boxes’) of a one-dimensional lattice and propagate according to some simple deterministic rules, as explained below. We start from an initial configuration of balls divided into L boxes, with at most one ball per box. The configuration at the next time step is obtained by letting a ‘carrier’ travel through the system from left to right. Doing so, each time the carrier passes over an occupied box and if it has not reached its maximum load l , it loads the ball and leaves the box empty. Each time the carrier carries at least one ball and passes over an empty box it unloads a ball in the box. An example is given in figure 1.³

Despite its apparent simplicity this model possesses stable solitons with nontrivial scattering under collisions. It has an infinity of conserved quantities, and its very rich mathematical and integrable structures have attracted a lot of interest. For example, the above combinatorial rule for the time evolution has its origin in the quantum R matrix at $q = 0$ as explained in appendix D (see [2] for a review).

An interesting family of problems arises when considering a statistical ensemble of random microscopic ball configurations [3–11]. In the simplest case the occupancies of the boxes can be taken to be independent and identically distributed (i.i.d.) random variables, and parameterized with a single parameter (the mean ball density). Such a statistical ensemble corresponds to an homogeneous and stationary state, and many quantities, like the densities of the various types of solitons and their associated mean velocities, can be computed exactly using the thermodynamic Bethe ansatz (TBA) [5, 11, 12].

It has also been shown that a hydrodynamic approach can accurately capture the long-time and large distance evolution of some inhomogeneous states. Due to the extensive number of conserved quantities in the model, the appropriate framework is the so-called generalized hydrodynamics (GHD). Introduced a few years ago [13–15], the GHD is based on the assumption that the system is locally in an homogeneous state with maximum entropy (generalized Gibbs ensemble (GGE) [16]) and the approach amounts to constructing and solving the set of continuity equations involving the local currents and local densities associated to the conserved quantities of an integrable system. It has been applied successfully to many integrable quantum and classical systems. On the classical side, we can mention for instance the application of GHD to the hard-rods model [17, 18], to the Toda model [19], to the sinh-Gordon model [20], to the BBS [10, 12] and to the (higher rank) complete BBS [21].

In the context of BBS, the evolution triggered by an initial domain-wall state with two different ball densities in the left half and the right half has been studied in details using GHD [12, 21]. In such a setup the BBS develops a series of plateaux in the variable $\zeta = x/t$ (space coordinate divided by time). The ball density and soliton content inside each plateau as well as the location ζ_0, ζ_1, \dots of the steps between consecutive plateaux could be determined exactly using GHD. In this domain-wall problem it has also been possible to go beyond the simplest

³The dynamics can also be defined on a periodic system by initializing the carrier load to some suitable value (proposition 5.1 of [2]).

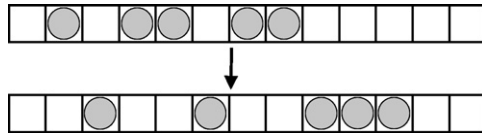


Figure 1. Top line: ball configuration. Bottom line: configuration at the next time step. We assumed here a carrier capacity $l \geq 3$.

hydrodynamic description by investigating some fluctuations effects. Due to the fact that the velocity of a given soliton is affected by the fluctuations of the densities of the other species of soliton, these velocities fluctuate and the step between two consecutive plateaux is not perfectly sharp but broadened. This broadening has a diffusive scaling and the width of the step number k behaves as $\delta x \simeq t^{1/2} \Sigma_k$ with constants Σ_k that have been calculated analytically. All these results for the domain wall problem have been also checked accurately using numerical simulations.

In the present work we are interested in the probability distribution of the number N_t of balls passing through the origin during a time t . We may take an initial domain wall state where the left half is an i.i.d. state with ball density $p_{\text{left}} > 0$, and the right half initially empty ($p_{\text{right}} = 0$). In such a case the number of transferred balls is also equal the number of balls in the right half at time t . But the ball propagation takes place only in the right direction and there is no ‘blocking effect’ from existing balls in the BBS dynamics. So, N_t does in fact not depend on the initial state in the right half of the system. The probability distribution of N_t is therefore the same (i) for the domain wall setup with ($p_{\text{left}} = p$ and $p_{\text{right}} = 0$) and (ii) in a uniform i.i.d. state with ball density $p_{\text{left}} = p_{\text{right}} = p$.

In the first step (section 2.2) we are interested in the second cumulant c_2 of N_t . The result is obtained by two different methods, by a direct calculation and with the TBA. Next (section 2.3) we compute the Drude weight, which is defined here in terms of the long-time limit of a spatially integrated current–current correlation. This correlation is formally similar to the one defining the second cumulant of N_t and the Drude weight is obtained using a TBA calculation which parallels that of the second cumulant.

A particularity of the model is to have a commuting family of temporal evolutions which are in duality with the conserved quantities⁴. In section 2.4 the currents associated with the conserved charges under the different temporal evolutions are introduced. These depend on one index associated to a conserved charge, and another one associated to a time evolution. The generalized current operators turn out to be symmetric under the exchange of the two indices, highlighting this duality. We compute the long-time limit of the correlations associated to these generalized currents. They generalize c_2 and D , and are shown to enjoy nontrivial symmetry relations among them. In section 2.5 we report on numerical calculations of the Drude weights and the generalized current correlations using microscopic simulations of the BBS, and a good agreement is found with the TBA results. In section 2.6 we compute the so-called flux Jacobian, which is a matrix playing an important role in GHD. The section 2.7 discusses another quantity defined in terms of spatially integrated current–current correlation, the variance of the total current. Contrary to the Drude weight the correlations are now taken at equal time, and this variance is obtained using a transfer matrix approach.

⁴ Although the commuting time evolutions should in principle be a common feature of integrable systems, their implementation can be quite involved in general. This is one reason why the BBS is a precious model, since it allows concrete descriptions of the different time evolution, as well as their simulations.

In the second part of the paper (section 3) we compute the scaled cumulants generating function (SCGF) associated to N_t . It characterizes all the cumulants of the probability distribution [22]. The Legendre transform of the SCGF, called large deviation rate function, describes not only the typical fluctuations around its mean value, but also the rare events. The large deviation rate function is compared with the results of numerical simulations. Finally, several results (second cumulant, Drude weight and SCGF) are generalized to a more complex GGE, with two temperatures (appendix C), one coupled to the total number of balls and the other one coupled to the total number of solitons.

2. Current correlations and Drude weights

We consider an i.i.d. homogeneous stationary state (characterized by some ball density $p = z/(z + 1) < 1/2$) and we study the probability distribution of the number N_t of balls crossing the origin between time 0 and time t , in the long time limit. The capacity of the carrier which induces the dynamics is denoted by l .

2.1. Mean current

The mean value of N_t grows linearly with time at a rate given by the mean ball current:

$$\langle N_t \rangle \sim t j^{(l)}. \tag{2.1}$$

The mean ball current $j^{(l)}$ is a simple function of the soliton currents $j_k^{(l)}$

$$j^{(l)}(z) = \sum_{k=1}^{\infty} k j_k^{(l)}. \tag{2.2}$$

The factor k above reflects the fact that each type- k solitons carries k balls. The mean soliton currents are products of the soliton velocities $v_k^{(l)}$ by the soliton densities ρ_k :

$$j_k^{(l)} = \rho_k v_k^{(l)}. \tag{2.3}$$

In integrable systems such densities can be obtained using the TBA [23]. This approach, applied to the BBS [5, 12], leads to a simple expression for the mean soliton densities in terms of the ball fugacity $z = p/(1 - p)$:

$$\rho_k = \frac{z^k(1 - z)^3(1 + z^{k+1})}{(1 + z)(1 - z^k)(1 - z^{k+1})(1 - z^{k+2})}. \tag{2.4}$$

As for the velocities, they obey a set of equations which reflect the fact that the mean velocity of each soliton species is affected by the collisions with the solitons of the other species. The essential ideas were proposed in [24–26], to describe soliton gases in the context of the Korteweg–de Vries and nonlinear Schrödinger equations. In the case of BBS the equation for the effective velocities reads [27] (see also [10, 12])

$$v_i^{(l)} = \kappa_i^{(l)} + \sum_{k=1}^{\infty} M_{i,k}(v_i^{(l)} - v_k^{(l)})\rho_k \quad (\forall i \geq 1), \tag{2.5}$$

where the bare soliton velocities are

$$\kappa_i^{(l)} = \min(i, l) \tag{2.6}$$

and the matrix M (with indices from $[1, \infty] \times [1, \infty]$) encoding the shifts experienced by solitons during collisions is

$$M_{i,k} = 2 \min(i, k). \tag{2.7}$$

For i.i.d. states these equations could be solved explicitly [12] and the following expression for the velocities were obtained:

$$v_k^{(l)} = \frac{1 + z^{l+1}}{1 - z^{l+1}} v_{\min(k,l)}, \quad v_k = \frac{1 + z}{1 - z} k - \frac{2z(1 + z)(1 - z^k)}{(1 - z)^2(1 + z^{k+1})}. \tag{2.8}$$

Remark: $v_k^{(\infty)} = v_k$. Combining the results above the mean ball current finally reduces to

$$j^{(l)}(z) = \frac{z}{1 - z} - (l + 1) \frac{z^{l+1}}{1 - z^{l+1}}. \tag{2.9}$$

2.2. Second cumulant

Next we are interested in the second cumulant of N_t , which turns out to be linear in t :

$$\langle \delta N_t^2 \rangle = \langle N_t^2 \rangle - \langle N_t \rangle^2 \sim t c_2. \tag{2.10}$$

This cumulant can be expressed as a time-integrated current–current correlation:

$$N_t = \int_0^t j(0, s) ds, \tag{2.11}$$

$$\langle \delta N_t^2 \rangle = \int_0^t \int_0^t ds ds' \langle j(0, s) j(0, s') \rangle^c \sim t c_2, \tag{2.12}$$

where $j(x, s)$ is the current flowing from the site $x - 1$ to the site x at time s . The superscript (l) specifying the dynamics T_l will often be omitted in what follows. A continuous time notation is used here for clarity, but the BBS is a discrete time model and $\int_0^t ds$ is in fact equivalent to $\sum_{s=0}^t$. In the carrier picture for BBS, $j(x, s)$ is nothing but the load of the carrier on this link. A general method to obtain such cumulants in integrable systems is described in [28, 29]. It applies when all the cumulants scale linearly in time. In what follows we apply this method to the case of the BBS, where it simplifies considerably.

2.2.1. Correlations and sum rules. We start from the general sum rule (A.12) derived in appendix A and specialize it to $f(x) = |x|$:

$$\sum_{x=-\infty}^{\infty} |x| \langle (n(x, t) - n(x, 0))(n(0, t) - n(0, 0)) \rangle^c = -2 \int_0^t \int_0^t ds ds' \langle j(0, s) j(0, s') \rangle^c. \tag{2.13}$$

Using the translation invariance (in space and time) of the correlators appearing in the lhs we get

$$\begin{aligned} \langle \delta N_t^2 \rangle &= \frac{1}{2} \sum_{x=-\infty}^{\infty} |x| (\langle n(x, t) n(0, 0) \rangle^c + \langle n(-x, t) n(0, 0) \rangle^c - 2 \langle n(x, 0) n(0, 0) \rangle^c) \\ &= \sum_{x=-\infty}^{\infty} |x| (\langle n(x, t) n(0, 0) \rangle^c - \langle n(x, 0) n(0, 0) \rangle^c). \end{aligned} \tag{2.14}$$

The equation above is essentially equivalent to (2.23) of [30] (see also (A.33) of [29]). The second cumulant is then expressed as

$$c_2 = \lim_{t \rightarrow \infty} \frac{1}{t} \sum_{x=-\infty}^{\infty} |x| (\langle n(x, t)n(0, 0) \rangle^c - \langle n(x, 0)n(0, 0) \rangle^c). \quad (2.15)$$

The connected equal time correlation $\langle n(x, 0)n(0, 0) \rangle^c$ vanishes for $x \neq 0$ in the i.i.d. state, so that

$$c_2 = \lim_{t \rightarrow \infty} \frac{1}{t} \sum_{x=-\infty}^{\infty} |x| \langle n(x, t)n(0, 0) \rangle^c. \quad (2.16)$$

Since the propagation only takes place in the right direction in the BBS, causality implies that the connected correlation $\langle n(x, t)n(0, 0) \rangle^c$ vanishes if $x < 0$ (for $t > 0$). So we have:

$$\sum_{x=-\infty}^{\infty} |x| \langle n(x, t)n(0, 0) \rangle^c = \sum_{x=-\infty}^{\infty} x \langle n(x, t)n(0, 0) \rangle^c. \quad (2.17)$$

We differentiate with respect to time, and use the local conservation law $\frac{d}{dt}n(x, t) = j(x, t) - j(x + 1, t)$:

$$\frac{d}{dt} \sum_{x=-\infty}^{\infty} |x| \langle n(x, t)n(0, 0) \rangle^c = \sum_{x=-\infty}^{\infty} x \langle (j(x, t) - j(x + 1, t))n(0, 0) \rangle^c \quad (2.18)$$

$$= \sum_{x=-\infty}^{\infty} \langle j(x, t)n(0, 0) \rangle^c = \sum_{x=-\infty}^{\infty} \langle j(0, 0)n(x, -t) \rangle^c. \quad (2.19)$$

We recognize the conserved charge $Q = \sum_{x=-\infty}^{\infty} n(x, -t)$ in the rhs, which means that (2.18) and (2.19) is independent of time. It can be evaluated at $t = 0$, or, instead, averaged over time. This yields two equivalent formulations of c_2 in terms of integrated current–density correlations:

$$c_2 = \sum_{x=-\infty}^{\infty} \langle j(x, 0)n(0, 0) \rangle^c \quad (2.20)$$

$$= \lim_{t \rightarrow \infty} \frac{1}{t} \int_0^t ds \sum_{x=-\infty}^{\infty} \langle j(x, s)n(0, 0) \rangle^c. \quad (2.21)$$

2.2.2. Direct calculation. In a GGE where β is the inverse temperature associated to the total number of balls (and $z = \exp(-\beta)$), (2.20) can be written as

$$c_2 = -\frac{\partial j}{\partial \beta} = z \frac{\partial j}{\partial z}. \quad (2.22)$$

Using (2.9) we directly obtain

$$c_2 = \frac{z}{(1-z)^2} - (l+1)^2 \frac{z^{l+1}}{(1-z^{l+1})^2}. \quad (2.23)$$

Table 1. Variance of the number of transferred balls for different values of the density p and capacity l . Comparison between (2.23) and numerical results (last column).

p	l	t	c_2 (2.23)	$\langle \delta N_t^2 \rangle / t$ numerics
0.2	4	6000	0.419 98	0.419
0.4	4	2000	1.633 52	1.63
0.3	10	2000	1.301 66	1.29

The above formula has been compared with numerical simulation of the BBS. The mean value and the second cumulant turn out to be in good agreement with the theoretical values (table 1). A generalization of this result to a two-temperature GGE is given in (C.13).

2.2.3. Second cumulant using TBA. We will now compute c_2 by a different approach. The total current J and the total number of balls Q can be decomposed into a mean value plus a fluctuating part: $J = Lj + \delta J$, $Q = Lp + \delta Q$. With these definitions (2.21) gives

$$c_2 = L^{-1} \lim_{t \rightarrow \infty} \frac{1}{t} \int_0^t ds \langle \delta J(s) \delta Q(0) \rangle. \quad (2.24)$$

The pseudoenergy $\epsilon_i = -\ln \left(\frac{2E_i - E_{i+1} - E_{i-1}}{L - 2E_i} \right)$ can be defined for each microscopic configuration, from the energies E_i , E_{i-1} and E_{i+1} . See appendix D or [12, equation (2.7)] for the explanation of E_i .⁵ These energies are conserved under the time evolution, and so are the pseudoenergies. The pseudoenergies can however fluctuate from configuration to configuration in a GGE. If we define $\delta \epsilon_i = L^{1/2}(\epsilon_i - \bar{\epsilon}_i)$, with $\bar{\epsilon}_i = \langle \epsilon_i \rangle$, these fluctuations have diagonal correlations [12]

$$\langle \delta \epsilon_i \delta \epsilon_j \rangle = \delta_{ij} (1 + e^{\bar{\epsilon}_i}) / \sigma_i, \quad (2.25)$$

where

$$\sigma_i = 1 - \sum_k M_{ik} \rho_k \quad (2.26)$$

is the hole density and M was given in (2.7).⁶ Note also that the expectation values of the pseudoenergies are given by $\bar{\epsilon}_i = -\ln(\rho_i / \sigma_i)$. The relation (2.25) was checked numerically (see table 2).

In turn, the fluctuations of the other quantities can be related to the fluctuations $\delta \epsilon_j$. In a large system $\delta J / L$ and $\delta Q / L$ are typically small, of order $\mathcal{O}(L^{-1/2})$, and we may linearize the relation between the ball density fluctuation and the pseudoenergies,

$$\delta Q / \sqrt{L} = \sum_{i=1}^{\infty} \delta \epsilon_i \frac{\partial \rho_b}{\partial \bar{\epsilon}_i}, \quad (2.27)$$

as well as the relation between the ball current density fluctuation and the pseudo energies

$$\delta J / \sqrt{L} = \sum_{i=1}^{\infty} \delta \epsilon_i \frac{\partial j_b}{\partial \bar{\epsilon}_i} + \dots \quad (2.28)$$

⁵The pseudoenergies can be used to write down the (fermionic) free energy $F = -\sum_k \ln(1 + e^{-\epsilon_k})$ [12, (3.15)] and the mode occupancies are $n_k = dF/d(\epsilon_k) = (1 + e^{\epsilon_k})^{-1} = (1 + 1/y_k)^{-1}$ with $y_k = e^{-\epsilon_k}$.

⁶The values of σ_i in the i.i.d. state are given by (C.4) with $a = z$ (or (3.25) in [12]).

Table 2. Pseudoenergy correlations for ball density $p = 0.4$: comparison between the TBA result (rhs of (2.25)), and numerical simulations (system size $L = 8 \times 10^4$ and average over $N_{\text{samples}} = 10^8$ configurations). The numerical results correspond to $L \left\langle \ln \left(\frac{2E_i - E_{i+1} - E_{i-1}}{L - 2E_i} \right) \ln \left(\frac{2E_j - E_{j+1} - E_{j-1}}{L - 2E_j} \right) \right\rangle^c$. As for the expectation values $\langle \epsilon_i \rangle$, the simulation results agree with $-\ln(\rho_i/\sigma_i)$ with very good accuracy (data not shown).

i	j	$\delta_{ij}(1 + e^{\epsilon_i})/\sigma_i$	$\langle \delta \epsilon_i \delta \epsilon_j \rangle$ numerics
1	1	8.012 82	8.0117
1	2	0	0.000 27
1	3	0	-0.000 79
2	2	27.2183	27.223
2	3	0	-0.0053
3	3	65.5367	65.588
4	4	131.789	132.07
5	5	238.454	239.37

In the equations above the ball density was denoted by ρ_b and the ball current by j_b . In (2.28) we have decomposed a current fluctuation, which is *not* conserved in time, in terms of fluctuations $\delta \epsilon_i$ of the pseudoenergies. Since each ϵ_i is a function of the $\{E_k\}$, the pseudoenergies and their fluctuations $\delta \epsilon_i$ are configuration-dependent but independent of time. So, by decomposing δJ over the $\delta \epsilon_i$ we have dropped all the time dependence in δJ and only the conserved component of the current has been kept (hence the dots in (2.28)). Following the idea of hydrodynamics projection onto the space of conserved quantities [15] we are here restricting ourselves to the part of the current which is constant in time and can be expressed in terms of the conserved energies. It is of course legitimate to do so in order to compute c_2 , thanks to the long-time limit in (2.24). Note that, in contrast, nothing was dropped in (2.27) since the total number of balls (and thus also δQ) is a conserved quantity.

Replacing (2.27), (2.28) and (2.25) in (2.24) yields

$$c_2 = \sum_{i=1}^{\infty} \frac{\partial \rho_b}{\partial \bar{\epsilon}_i} \frac{\partial j_b}{\partial \bar{\epsilon}_i} \frac{1 + e^{\bar{\epsilon}_i}}{\sigma_i}. \quad (2.29)$$

What remains to be done is to compute the derivatives $\frac{\partial \rho_b}{\partial \bar{\epsilon}_i}$ and $\frac{\partial j_b}{\partial \bar{\epsilon}_i}$.

Once the pseudoenergies associated to the GGE are known we can introduce the ‘dressing’ operation, which is standard in the framework of TBA. A set of quantities o_i labelled by some index $i \in [1, \infty]$ representing a soliton size can be grouped into a column vector $o = (o_1, o_2, \dots)$. We then define the ‘dressing matrix’ G and construct a new dressed vector o^{dr} [12]:

$$o^{\text{dr}} = Go, \quad (2.30)$$

$$G = (1 + M\hat{y})^{-1}, \quad (2.31)$$

where \hat{y} is the diagonal matrix with elements $y_j = \exp(-\bar{\epsilon}_j)$.⁷

⁷ The diagonal entries of the matrix M do not enter the velocity equation (2.5) and there is therefore some freedom to redefine its diagonal part. This leads to some freedom in the definition of the dressing operation and the present choice (also used in [12]) is not the same as in [15]. With (2.31) we have $o^{\text{dr}} = o - M\hat{y}o^{\text{dr}}$. In [15] the dressing operation (denoted with a prime) is instead defined by $o^{\text{dr}'} = o + T\hat{n}o^{\text{dr}'}$ where $T = 1 - M$ and \hat{n} is the diagonal matrix with

The basic relations that will be used in the following calculation are

$$y_i = e^{-\bar{\epsilon}_i} = \frac{\rho_i}{\sigma_i}, \quad \sigma_i v_i^{(l)} = (G\kappa^{(l)})_i \quad (= (\kappa^{(l)\text{dr}})_i). \quad (2.32)$$

From $G + GM\hat{y} = \text{Id}$, we find that GM is symmetric:

$$GM = \hat{y}^{-1} - G\hat{y}^{-1} = \hat{y}^{-1} - (\hat{y} + \hat{y}M\hat{y})^{-1} = (GM)^t. \quad (2.33)$$

Its (i, j) element is concretely expressed as

$$(GM)_{ij} = 2 \sum_k G_{ik} \min(k, j) = 2(G\kappa^{(j)})_i = 2\sigma_i v_i^{(j)}, \quad (2.34)$$

where the invariance of the last expression under the interchange $i \leftrightarrow j$ can also be confirmed at the level of explicit formulae, see (2.72). Using $\frac{\partial y_n}{\partial \bar{\epsilon}_i} = -\delta_{in} y_i$, we get

$$\begin{aligned} \frac{\partial G_{jk}}{\partial \bar{\epsilon}_i} &= - \sum_{m,n} G_{jm} \frac{\partial (M\hat{y})_{mn}}{\partial \bar{\epsilon}_i} G_{nk} = \sum_m G_{jm} M_{mi} y_i G_{ik} \\ &= (GM)_{ji} y_i G_{ik} = (GM)_{ij} y_i G_{ik} = 2\sigma_i v_i^{(j)} y_i G_{ik} = 2\rho_i v_i^{(j)} G_{ik}. \end{aligned} \quad (2.35)$$

Let us introduce $\eta_j^{(l)}$, which includes, due to $v_k^{(l=1)} = 1$, the density and the current of balls as special cases:

$$\eta_j^{(l)} = \sum_k \min(j, k) \rho_k v_k^{(l)}, \quad \eta_\infty^{(1)} = \rho_b, \quad \eta_\infty^{(l)} = j_b. \quad (2.36)$$

It is expressed in terms of G as

$$\begin{aligned} \eta_j^{(l)} &= \sum_k \min(j, k) y_k \sigma_k v_k^{(l)} = \frac{1}{2} \sum_k (M\hat{y})_{jk} (G\kappa^{(l)})_k \\ &= \frac{1}{2} \sum_k (-\text{Id} + G^{-1})_{jk} (G\kappa^{(l)})_k = -\frac{1}{2} \sum_k G_{jk} \kappa_k^{(l)} + \frac{1}{2} \kappa_j^{(l)} = \eta_l^{(j)}, \end{aligned} \quad (2.37)$$

where the last equality is due to the symmetry (2.33). The symmetry of η under the exchange of the upper and lower indices will play an important role in section 2.4. By means of (2.35), the $\bar{\epsilon}_i$ derivative is calculated as

$$\frac{\partial \eta_j^{(l)}}{\partial \bar{\epsilon}_i} = -\frac{1}{2} \sum_k \frac{\partial G_{jk}}{\partial \bar{\epsilon}_i} \kappa_k^{(l)} = -\sum_k \rho_i v_i^{(j)} G_{ik} \kappa_k^{(l)} = -\rho_i \sigma_i v_i^{(j)} v_i^{(l)}. \quad (2.38)$$

From this with $j = \infty$ and (2.36) it follows that

$$\frac{\partial \rho_b}{\partial \bar{\epsilon}_i} = -\rho_i \sigma_i v_i^{(\infty)}, \quad (2.39)$$

$$\frac{\partial j_b}{\partial \bar{\epsilon}_i} = -\rho_i \sigma_i v_i^{(\infty)} v_i^{(l)}. \quad (2.40)$$

entries $n_i = \rho_i / (\sigma_i + \rho_i)$. The two dressing definitions lead to the same effective soliton speeds $v_i^{(l)} = \kappa_i^{(l\text{dr}} / (1^{\text{dr}})_i = \kappa_i^{(l\text{dr}'} / (1^{\text{dr}'})_i$ and can both be used to obtain physical quantities.

The results (2.39) and (2.40) can be inserted into (2.29):

$$c_2 = \sum_{i \geq 1} \rho_i \sigma_i (\rho_i + \sigma_i) (v_i^{(\infty)})^2 v_i^{(l)}. \quad (2.41)$$

This expression can be checked to agree with (2.23).

2.3. Drude weights

The Drude weight is an important quantity in the field of transport. This linear response coefficient characterizes the increase of the current in presence of a force which couples to the charges. The recent years have seen very important progress in the understanding of this quantity in one-dimensional integrable systems [31–36]. D can be defined in terms of a time average current–current correlation function⁸:

$$D = \lim_{t \rightarrow \infty} \frac{1}{t} \int_0^t ds \sum_x \langle j(x, s) j(0, 0) \rangle^c. \quad (2.43)$$

Noting the close similarity with (2.21), we repeat the hydrodynamic projection of the current fluctuations onto the pseudoenergy fluctuations, which lead to (2.29). It yields to

$$D = \sum_{i=1}^{\infty} \left(\frac{\partial j_b}{\partial \bar{\epsilon}_i} \right)^2 \frac{1 + e^{\bar{\epsilon}_i}}{\sigma_i} \quad (2.44)$$

and the derivatives $\frac{\partial j_b}{\partial \bar{\epsilon}_i}$ are again given by (2.40). We thus obtain a TBA expression for the Drude weight

$$D = \sum_{i \geq 1} \rho_i \sigma_i (\rho_i + \sigma_i) (v_i^{(\infty)} v_i^{(l)})^2. \quad (2.45)$$

The expression for the density correlation $R = \sum_x \langle n(x, t) n(0, 0) \rangle^c$ has a form similar to that of c_2 and D . Thanks to the conservation of the total number of balls R is independent of time and in an i.i.d. state it is trivially equal to $p(1 - p)$. Following the reasoning leading to (2.41) and (2.45) we get

$$p(1 - p) = \sum_{i \geq 1} \rho_i \sigma_i (\rho_i + \sigma_i) (v_i^{(\infty)})^2. \quad (2.46)$$

For more details about the above formula and their expression in matrix forms we refer the readers to section 2.6.3. The structure of these formulae is very similar to the results for c_2 and D in the Lieb–Liniger model, obtained by Doyon and Spohn (equations (1.2) and (1.3) of [33]). In the latter work a central idea is to implement the long-time limit in the definition of D via the hydrodynamic projection (see (2.18) of [33]). This approach amounts to projecting the observable of interest (for D , the current) via a suitable scalar product into the time-invariant subspace, spanned by the conserved charges. As mentioned in the paragraph before (2.29), in

⁸ Using the sum rule (A.12) with the choice $f(x) = x^2$, (2.43) can also be written

$$D = \lim_{t \rightarrow \infty} \frac{1}{t^2} \sum_x x^2 \langle n(x, t) n(0, 0) \rangle^c, \quad (2.42)$$

which is another useful definition of D .

the approach presented here the projection is implemented by decomposing the current fluctuation over the conserved variables ϵ_i . The relation (2.25) shows that the pseudoenergies form a convenient orthogonal basis in the subspace of conserved quantities.

Aided by some computer algebra system it was possible to obtain explicit formulae for the Drude weight as a function of z for a few values of the carrier capacity l , denoted by $D^{(l)}$:

$$D^{(2)} = \frac{z(1-z)(1-z^2)^3(1+11z+11z^3+z^4)}{(1-z^3)^3(1-z^4)}, \tag{2.47}$$

$$D^{(3)} = \frac{z(1-z)(1-z^2)^2(1-z^3)}{(1-z^4)^3(1-z^6)} \times (1+11z+44z^2+29z^3+30z^4+29z^5+44z^6+11z^7+z^8), \tag{2.48}$$

$$D^{(4)} = \frac{z(1-z)^2(1-z^3)}{(1-z^5)^3(1-z^6)(1-z^8)} \times (1+10z+35z^2+117z^3+68z^4+254z^5+95z^6+357z^7+126z^8+357z^9+95z^{10}+254z^{11}+68z^{12}+117z^{13}+35z^{14}+10z^{15}+z^{16}), \tag{2.49}$$

$$D^{(5)} = \frac{z(1-z)(1-z^2)^2(1-z^4)(1-z^5)}{(1-z^6)^3(1-z^8)(1-z^{10})} \times (1+11z+44z^2+140z^3+355z^4+406z^5+480z^6+443z^7+633z^8+714z^9+896z^{10}+714z^{11}+633z^{12}+443z^{13}+480z^{14}+406z^{15}+355z^{16}+140z^{17}+44z^{18}+11z^{19}+z^{20}). \tag{2.50}$$

The functions above as well as $D^{(\infty)}$ are plotted as a function of the ball density $p = z/(1+z)$ in figure 2. When the density is slightly below 0.5 we note a rapid increase of the Drude weight with l . Since l acts as a cutoff on the effective speed of the solitons of size $k \geq l$, this indicates that the large solitons have a dominant contribution to the Drude weight.

Going further one can obtain an expression for $D^{(l)}$ for generic l with finite number of terms. To this end we first set $W_i = \rho_i \sigma_i (\rho_i + \sigma_i) v_i^2$. Then we have

$$\sum_{i < l} W_i = \frac{zA_l}{(1+z)^2(1-z)^2(1-z^{l+1})^2}, \tag{2.51}$$

$$A_l = 1 + 3z^{2l} + 8z^{2l+1} + 3z^{2l+2} + z^{4l+2} - (l+1)^2(z^{l+2} + z^{3l}) + (l^2 - 4)(z^{l+1} + z^{3l+1}) + (l-1)(l+3)(z^l + z^{3l+2}) - l^2(z^{l-1} + z^{3l+3}).$$

Note that $A_0 = A_1 = 0$ indeed holds. It leads to

$$D^{(1)} = \sum_{i \geq 1} W_i (v_i^{(1)})^2 = \sum_{i \geq 1} W_i = \frac{zA_\infty}{(1+z)^2} = \frac{z}{(1+z)^2}. \tag{2.52}$$

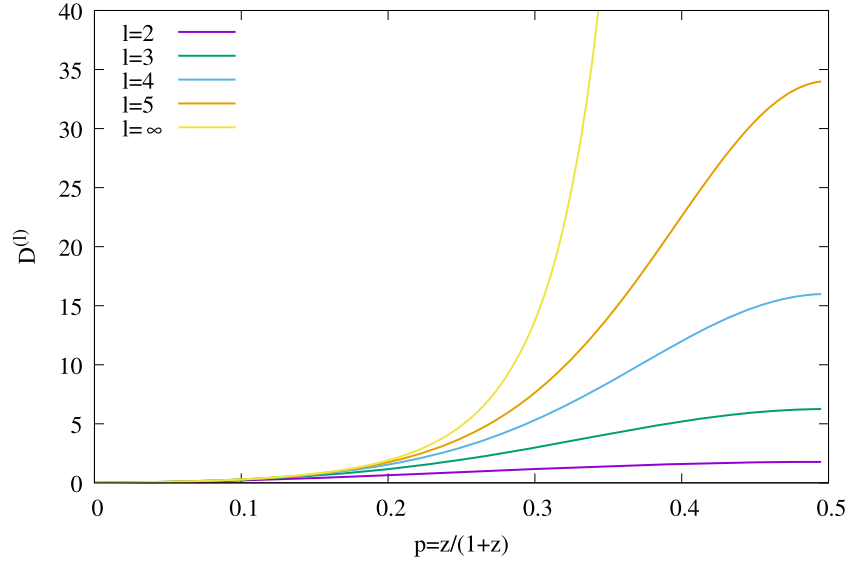


Figure 2. Drude weight $D^{(l)}$ for $l = 2, 3, 4, 5$ and $l = \infty$, plotted as a function of the ball density p . For $l \geq 2$ the Drude weight is linear in p at low density: $D^{(l)} = p + 11p^2 + \mathcal{O}(p^3)$.

By means of this, the infinite sum (2.45) is reduced to a finite one as

$$D^{(l)} = \sum_{i < l} W_i (v_i^{(l)})^2 + (v_l^{(l)})^2 \sum_{i \geq l} W_i \tag{2.53}$$

$$= \sum_{i < l} W_i (v_i^{(l)})^2 + (v_l^{(l)})^2 \left(\frac{z}{(1+z)^2} - \sum_{i < l} W_i \right), \tag{2.54}$$

where the second term is known by (2.51). Or equivalently,

$$D^{(l)} = \left(\frac{1+z^{l+1}}{1-z^{l+1}} \right)^2 \left(\sum_{i < l} W_i (v_i^2 - v_l^2) + v_l^2 \frac{z}{(1+z)^2} \right). \tag{2.55}$$

We note that in the half filled limit the Drude weight tends to a simple value

$$\lim_{z \rightarrow 1} D^{(l)} = \left(\frac{l(l+2)}{6} \right)^2. \tag{2.56}$$

This is consistent with the observation that $D^{(\infty)}$ diverges when $z \rightarrow 1$ (see figure 2). To conclude this section we mention that some generalization of these results to a two-temperature GGE is discussed in appendix C.

2.4. Generalized current correlations and their symmetries

Thus far we have considered c_2 (2.24), D (2.43) and R (2.46). They are all associated with the number balls, which is one special case E_∞ of the conserved quantities E_j with $j = 1, 2, \dots$ [12]. Here we discuss a natural generalization corresponding to the whole family $\{E_j\}$.

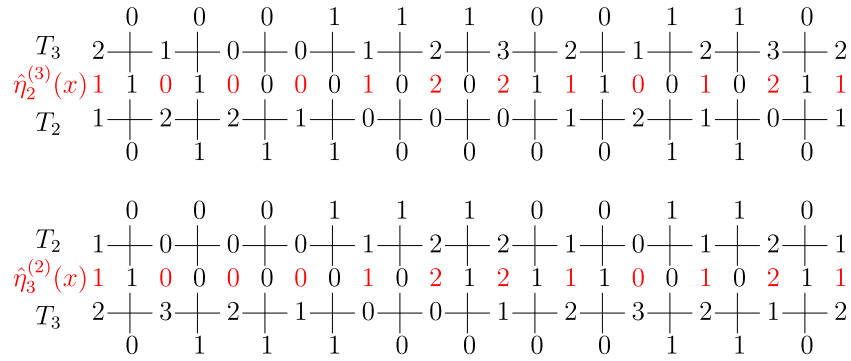


Figure 3. Top: the generalized current $\eta_2^{(3)}(x)$ is shown in red letters. According to (D.7) and (D.3), it is evaluated as $\min(2 - \alpha_1, \beta_1)$, where α_1 and β_1 are numbers just under and above it, respectively. Bottom: similarly, the generalized current $\eta_3^{(2)}(x)$ is defined using $\min(3 - \alpha_1, \beta_1)$. One can see on this example that the two currents densities are in fact equal: $\eta_2^{(3)}(x) = \eta_3^{(2)}(x)$.

Let us denote by $\hat{\eta}_j^{(l)}(x)$ the microscopic operator measuring the current associated to the j th energy, under the time evolution T_l , and at position x . To define this operator microscopically in a given state s of the BBS we need to consider two successive time evolutions $s \rightarrow T_l(s) \rightarrow T_i T_l(s)$, as illustrated in figure 3. Consider the carrier inducing the first T_l and let $u(x) = (u_0, u_1)$ be its state at position x , where u_0 and u_1 are the numbers of empty space and balls in it, respectively. Similarly, let $u'(x) = (u'_0, u'_1)$ be the state of another carrier for the second time evolution T_i at position x . By the definition of the carrier capacity $u_0 + u_1 = l$ and $u'_0 + u'_1 = i$. Now $\hat{\eta}_i^{(l)}(x)$ of the state s is defined by $\hat{\eta}_i^{(l)}(x) = \min(u'_0, u_1)$ (red integers in figure 3). By extending the argument in section 2.2 in [12], it can be shown that these generalized currents are in fact symmetric in the two capacities l and i : $\hat{\eta}_i^{(l)}(x) = \hat{\eta}_l^{(i)}(x)$, and $\hat{\eta}_\infty^{(l)}(x) = j^{(l)}(x)$ and $\hat{\eta}_k^{(1)}(x) =$ local term for the energy E_k . We refer the reader to appendix D for more details about the construction of these currents.

The mean values of these energy currents are expressed in terms of $\eta_j^{(l)}$ (2.36) as

$$\eta_j^{(1)} = \langle \hat{\eta}_j^{(1)} \rangle = \sum_{k \geq 1} \min(j, k) \rho_k, \quad \eta_j^{(l)} = \langle \hat{\eta}_j^{(l)} \rangle = \sum_{k \geq 1} \min(j, k) \rho_k v_k^{(l)}, \quad (2.57)$$

where $v_k^{(l=1)} = 1$ is used. The mean ball current (2.2) corresponds to $\eta_\infty^{(l)}$, and the ball density is $\eta_\infty^{(1)}$. Comparing (2.57) and (2.36), we see that the index l allows interpolating between the density and the current, utilizing the variety of time evolutions in the system.

Now consider the time-averaged correlation

$$\mathcal{C}_{i,j}^{m,l,n} = \lim_{t_n \rightarrow \infty} \frac{1}{t_n} \int_0^{t_n} ds \sum_x \langle \hat{\eta}_i^{(m)}(x, s) \hat{\eta}_j^{(l)}(0, 0) \rangle^c, \quad (2.58)$$

which is also expected to coincide with the limit

$$\mathcal{C}_{i,j}^{m,l,n} = \lim_{t_n \rightarrow \infty} \sum_x \langle \hat{\eta}_i^{(m)}(x, t_n) \hat{\eta}_j^{(l)}(0, 0) \rangle^c. \quad (2.59)$$

In the definitions above we have denoted the time variable by t_n to emphasize that the time evolution from time 0 to time t_n is computed with T_n . We however conjecture that, for sufficiently

large n this quantity becomes independent of n , and we set

$$C_{i,j}^{l,m} = \lim_{n \rightarrow \infty} C_{i,j}^{m,l,n}. \tag{2.60}$$

This property is easy to check if at least one of the indices m, l, i, j is equal to one. Using the symmetry between the upper and lower indices in $\hat{\eta}_i^{(l)}$, the index which is equal to one can be moved to an upper position. The correlation (2.59) can then be formulated using, say, $\sum_x \hat{\eta}_i^{(1)}(x)$, which is the conserved energy E_i . The time evolution therefore drops and $C_{i,j}^{m,l,n}$ appears to be independent of n in such a case. As we will see in section 2.5, in more general cases the numerical simulations support the fact that $C_{i,j}^{m,l,n}$ is independent of n for $n \geq \min(m, l)$.

The family of generalized correlations $C_{i,j}^{l,m}$ includes three quantities we have defined previously:

$$c_2 = C_{\infty,\infty}^{1,l}, \quad D = C_{\infty,\infty}^{l,l}, \quad R = C_{\infty,\infty}^{1,1}. \tag{2.61}$$

As seen here, the superscripts l, m in (2.60) are restricted to 1 (for density) or l (for current) in the original setting. However, keeping them general reveals an interesting symmetry of the problem as we see below. Admitting the validity of the previous TBA argument leads to

$$C_{i,j}^{l,m} = \sum_{k=1}^{\infty} \frac{\partial \eta_i^{(l)}}{\partial \bar{\epsilon}_k} \frac{\partial \eta_j^{(m)}}{\partial \bar{\epsilon}_k} \frac{1 + e^{\bar{\epsilon}_k}}{\sigma_k} \tag{2.62}$$

$$= \sum_{k \geq 1} \rho_k \sigma_k (\rho_k + \sigma_k) v_k^{(i)} v_k^{(j)} v_k^{(l)} v_k^{(m)}. \tag{2.63}$$

It tells that $C_{i,j}^{l,m}$ is *completely symmetric in the four indices*.

The symmetry relating $C_{i,j}^{l,m}$ to $C_{i,j}^{i,m}$ and $C_{i,j}^{l,j}$ derives from the equality $\hat{\eta}_i^{(l)} = \hat{\eta}_l^{(i)}$. For example, the ball density correlation $R = C_{\infty,\infty}^{1,1}$ coincides with $C_{1,1}^{\infty,\infty}$ which is the soliton current correlation under the time evolution T_∞ . In this particular case the symmetry can be checked directly at the microscopic level⁹.

The symmetry relating $C_{i,j}^{l,m}$ to $C_{j,i}^{m,l}$ follows from the fact that, in the correlation $\langle \hat{\eta}_i^{(m)}(x, s) \hat{\eta}_j^{(l)}(0, 0) \rangle^c$ one can replace (x, s) by $(-x, -s)$. The possibility to exchange, say, the indices l and m in $C_{i,j}^{l,m}$ is apparent in the TBA result (2.63) but it does not follow from a simple microscopic symmetry. It will be interesting to seek such an enhanced symmetry among the transport characteristics also in other integrable models admitting the GHD approach.

We note that the family of characteristics $C_{\infty,\infty}^{m,l}$ ($m = 1, 2, \dots, l$) interpolating c_2 and D in (2.61) are all expressible as a finite sum similar to (2.54):

$$C_{\infty,\infty}^{m,l} = \sum_{k < m} W_k v_k^{(l)} (v_k^{(m)} - v_m^{(m)}) + c_2 v_m^{(m)}. \tag{2.64}$$

⁹To this end one compares the 1-energy density (or soliton density) $e_1(x, t)$ at times t and $t + 1$ (according to the T_∞ evolution) to deduce the associated current $j_1(x, t)$ satisfying the discrete continuity equation $e_1(x, t + 1) - e_1(x, t) + j_1(x + 1/2, t) - j_1(x - 1/2, t) = 0$. Doing so one realizes that the soliton current is identical to the ball density, up to a half lattice spacing shift: $j_1(x, t) = n(x - 1/2, t)$. This explains the equality between their correlations and provides an explicit check of the general symmetry mentioned above.

When i, j, l, m are all finite, $C_{i,j}^{l,m}$ is evaluated as a rational function by means of (C.15) with $a = z$ as

$$C_{i,j}^{l,m} = \sum_{k < r} \rho_k \sigma_k (\rho_k + \sigma_k) v_k^{(i)} v_k^{(j)} v_k^{(l)} v_k^{(m)} + \frac{z^r (1-z)^4 (1+z^{2r+1})}{(1+z)^3 (1-z^r)^2 (1-z^{r+1})^2} v_i^{(i)} v_j^{(j)} v_l^{(l)} v_m^{(m)}, \tag{2.65}$$

where $r = \max(i, j, l, m)$.

2.5. Numerical calculation of the Drude weights

In this section we present some direct numerical calculations of the correlation $C_{i,j}^{m,l,n}$. The results are displayed in figures 4–6.

Figure 4 illustrates the dependence of $C_{i,j}^{m,l,n}$ on the dynamical parameter n in the case $m = l$ and $i = j = 99$ (almost ∞). Since T_1 is a simple translation we have $\hat{\eta}_i^{(l)}(x, t_1) = \hat{\eta}_j^{(l)}(x - t_1, 0)$ and (2.59) reduces to an equal-time correlation when $n = 1$ (no long-time limit). This equal-time current–current correlation is computed in section 2.7 and the numerical data for $n = 1$ agree with the analytical result. For general values of n we can compare the numerical results for $C_{\infty,\infty}^{l,l,n}$ with the Drude weight $C_{\infty,\infty}^{l,l}$, and the data plotted in figure 4 suggest that we have $C_{\infty,\infty}^{l,l,n} = C_{\infty,\infty}^{l,l}$ for $n \geq l$. We are however unaware of a method to obtain $C_{\infty,\infty}^{l,l,n}$ in the intermediate regime $1 < n < l$.

Figure 5 illustrates the dependence on the dynamical parameter n in a case where $m \neq l$ (and still $i = j = 99$). For $n = 1$ the correlation $C_{\infty,\infty}^{m,l,1}$ is again an equal-time correlation between two generalized currents. For larger values of the dynamical parameter n the data displayed in figure 5 suggest that we have $C_{\infty,\infty}^{m,l,n} = C_{\infty,\infty}^{m,l}$ for $n \geq \min(m, l)$, even though we have no proof.

Finally, figure 6 illustrates the convergence of current–current correlations as a function of time and for different time evolutions. This figure shows that it converges to $C_{\infty,\infty}^{l,l,n}$ after only a relatively short relaxation time. In this particular example ($l = 5$ and ball density $p = 0.3$) the relaxation time appears to decrease when n increases. As for the long-time limit of the correlator, it coincides with the TBA expression (2.63) only for $n \geq l = 5$, in agreement with the conjectured proposed above.

If the long-time limit of a current–current correlation (that is, the Drude weight) is subtracted, the time integral of the remaining part of the correlation is an element of the Onsager matrix, which characterizes the diffusive corrections to the hydrodynamics [15, 36]. We see from figure 6 that such Onsager coefficient would be dominated by a few short-time value of the correlator. The detailed study of the Onsager matrix in the BBS is left for future studies¹⁰.

In the hydrodynamic projection scheme the Drude weights and its generalizations (2.59) depend on the projections of the current operators onto the space spanned by the conserved quantities. The energies E_i are conserved whatever the dynamical parameter n and their contribution to the long-time limit of the current–current correlations was included in (2.63), via the pseudoenergy variables. However, the numerical observation that $C_{i,j}^{m,l,n}$ can be different from (2.63) suggest that T_n may not always be sufficiently mixing inside each energy sector fixed by the $\{E_i\}$ data, in particular for small n . This is obvious for $n = 1$ (no mixing at all), but as a less trivial example consider two solitons of sizes p and p' under the evolution T_n , with $n \leq p < p'$. Because the effective soliton velocities (2.8) are independent of the soliton size when they are larger than n the mean distance between two big solitons will be almost constant in time (up to

¹⁰The diffusive broadening of density steps in a domain-wall problem was studied analytically and numerically for the BBS in [12, 21].

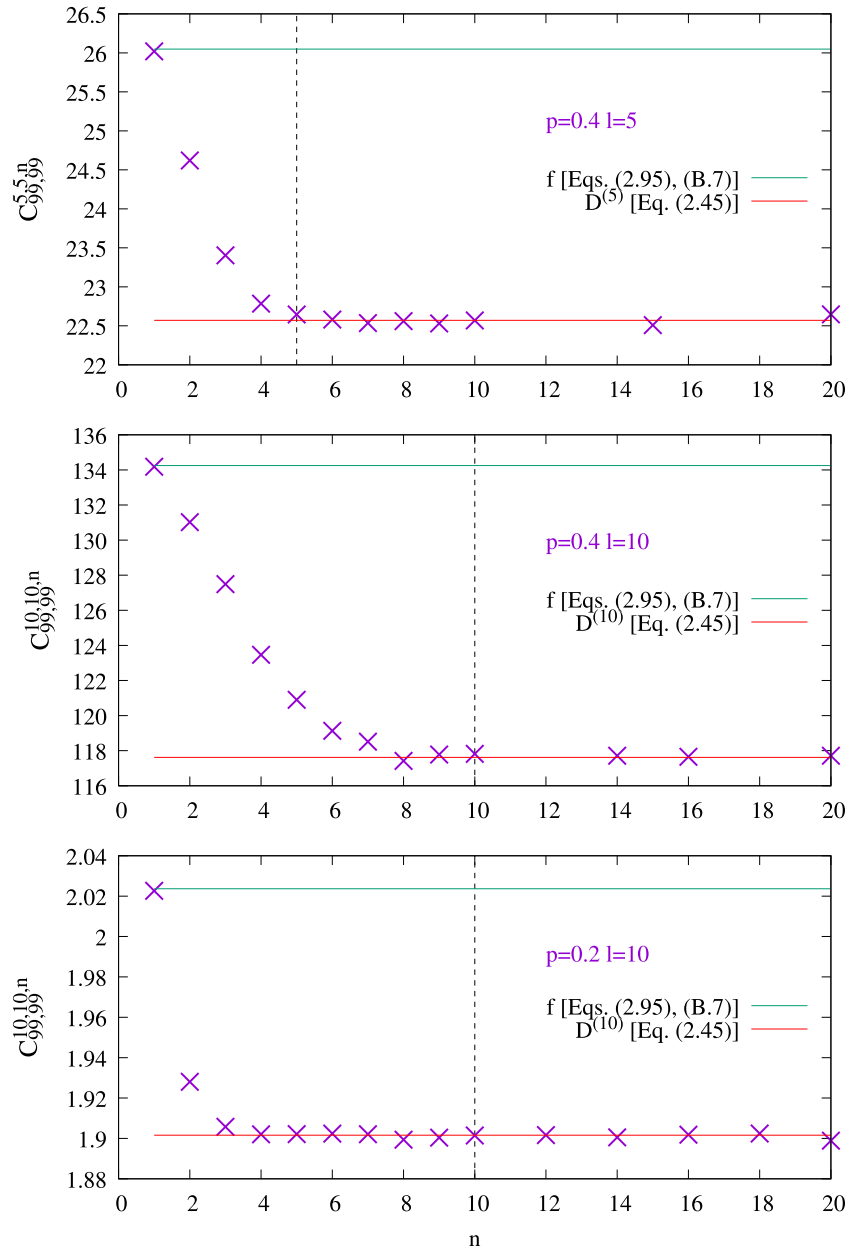


Figure 4. Numerical results for the Drude weight $C_{99,99}^{l,l,n}$ (2.59) for different values of the ball densities ($p = 0.4$ and $p = 0.2$), two values of l and different values of the parameter n characterizing the time evolution. The simulations were carried out on a periodic system of size $L = 60\,000$, with time $t_n = 1000$ and $N_{\text{samples}} = 5 \times 10^5$ random initial configurations (top and middle panel) and with $N_{\text{samples}} = 8 \times 10^6$ in the bottom panel. The red horizontal lines represent the TBA result (2.45) and the green lines represent (B.7).

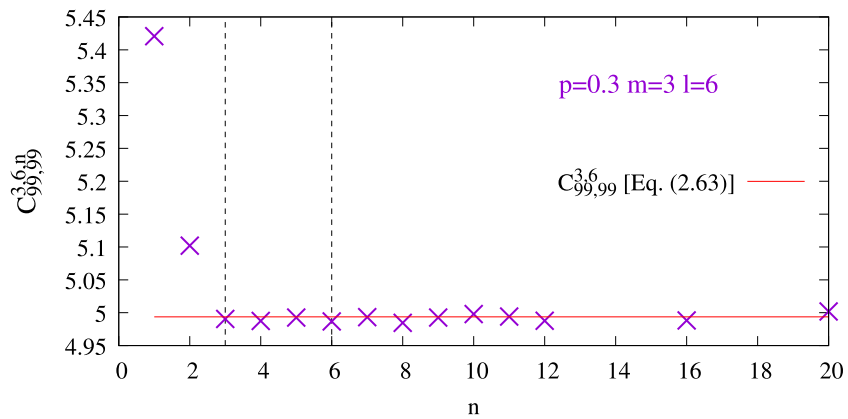


Figure 5. Numerical results for $C_{99,99}^{3,6,n}$ (2.59) plotted as a function of n . The data suggests that $C_{\infty,\infty}^{m,l,n}$ coincides with the TBA result (2.63) for $C_{\infty,\infty}^{m,l}$ when $n \geq \min(m, l)$. Simulations performed with (periodic) system size $L = 30\,000$, time $t_n = 1000$ and 1.5×10^6 random initial conditions with ball density $p = 0.3$.

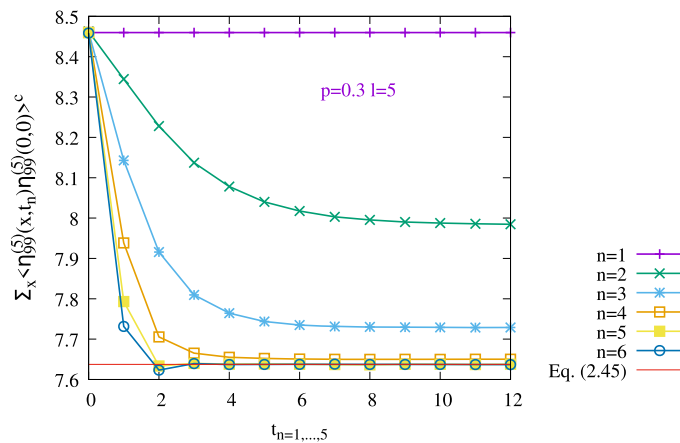


Figure 6. Correlation $\sum_x \langle \eta_{99}^{(5)}(x, t_n) \eta_{99}^{(5)}(0, 0) \rangle^c$ plotted as a function of time for different time evolutions T_n . Since T_1 is a simple translation the dynamics is trivial and the correlation is independent of time (purple curve, $n = 1$). For $n \geq 2$ the dynamics is however nontrivial, and the correlation relaxes to a finite value at sufficiently long times. For $n \geq 5$ this long-time limit coincides with the TBA value (2.45) (horizontal red line). Simulations performed with (periodic) system size $L = 20\,000$, and 36×10^6 random initial conditions with ball density $p = 0.3$.

small fluctuations due to the collisions with smaller and slower solitons). This may be a hint why some minimal value of n seems required for a current–current correlation to converge to the TBA result (2.63).

2.6. Flux Jacobian and related matrices

In this section we present concrete forms of the flux Jacobians corresponding to the commuting family of time evolutions in our BBS. We will also describe the relations with the matrices of 2nd cumulants and the Drude weights, as well as their generalization $C_{i,j}^{l,m}$.

2.6.1. Normal modes. In BBS, the role of the conserved charge q_i and the current j_i in the flux Jacobian [15, equation (26)] are played by $\eta_i^{(1)}$ and $\eta_i^{(l)}$ if the time evolution is taken as T_l . From [12, equation (3.9)], $\eta_i^{(1)}$ is related to the hole density as $\sigma_i = 1 - 2\eta_i^{(1)}$. The associated conserved currents for the time evolution T_l are given by $\sigma_i v_i^{(l)}$. Therefore, we have the equations of conservation:

$$\partial_t \sigma_i + \partial_x (\sigma_i v_i^{(l)}) = 0. \quad (2.66)$$

We use the fact that σ_i and $v_i^{(l)}$ are functions of y_j given by $\sigma_i = \sum_{k=1}^{\infty} G_{ik}$ and $\sigma_i v_i^{(l)} = (G\kappa^{(l)})_i = (GM)_{il}/2$. Their partial derivatives with respect to y_j are calculated as

$$\frac{\partial \sigma_i}{\partial y_j} = -\sum_k y_j^{-1} \frac{\partial G_{ik}}{\partial \bar{\epsilon}_j} = -\sum_k y_j^{-1} 2\sigma_j v_j^{(i)} y_j G_{jk} = -2\sigma_j^2 v_j^{(i)} = -(GM)_{ij} \sigma_j, \quad (2.67)$$

$$\frac{\partial (\sigma_i v_i^{(l)})}{\partial y_j} = -\frac{1}{2} \sum_k y_j^{-1} \frac{\partial G_{ik}}{\partial \bar{\epsilon}_j} M_{kl} = -\sum_k y_j^{-1} \sigma_j v_j^{(i)} y_j G_{jk} M_{kl} = -2\sigma_j^2 v_j^{(i)} v_j^{(l)} = -(GM)_{ij} \sigma_j v_j^{(l)}, \quad (2.68)$$

where (2.35) is used. Substituting them into (2.66), we deduce that y_j are normal modes [12, equation (5.20)]:

$$\partial_t y_j + v_j^{(l)} \partial_x y_j = 0. \quad (2.69)$$

2.6.2. Family of flux Jacobians. Let us introduce the infinite dimensional matrices

$$V = (v_j^{(i)})_{i,j \geq 1}, \quad V_d^{(l)} = \text{diag}(v_1^{(l)}, v_2^{(l)}, \dots), \quad \hat{\sigma} = \text{diag}(\sigma_1, \sigma_2, \dots), \quad (2.70)$$

where the effective velocity is related to the hole density [12, equation (4.19)] as

$$v_i^{(l)} = \sum_{k=1}^{\min(l,i)} \frac{\sigma_l}{\sigma_{k-1} \sigma_k} \quad (2.71)$$

with $\sigma_0 = 1$. We therefore have an explicit expression of the hole currents

$$j_i^{(l)\text{hole}} = \sigma_i v_i^{(l)} = \sum_{k=1}^{\min(l,i)} \frac{\sigma_i \sigma_l}{\sigma_{k-1} \sigma_k} \quad (2.72)$$

in terms of the hole densities σ_i . In the GHD context such an expression is an equation of state [15, equation (22)]. The results (2.67) and (2.68) are expressed in matrix forms as

$$\frac{\partial \sigma}{\partial y} = -GM\hat{\sigma}, \quad \frac{\partial (\sigma v^{(l)})}{\partial y} = -GMV_d^{(l)}\hat{\sigma}. \quad (2.73)$$

If we use σ_i as variables to express the currents, (2.66) is written as

$$\partial_t \sigma_i + \sum_{j=1}^{\infty} A_i^{(j)} \partial_x \sigma_j = 0. \tag{2.74}$$

The matrix $A^{(l)} = (A_i^{(j)})_{i,j \geq 1}$ (row i , column j) is the flux Jacobian, where

$$A_i^{(j)} = \frac{\partial(\sigma_i v_i^{(l)})}{\partial \sigma_j} = \sum_k \frac{\partial(\sigma_i v_i^{(l)})}{\partial y_k} \frac{\partial y_k}{\partial \sigma_j}. \tag{2.75}$$

In terms of matrices in (2.73) this is equivalent to

$$A^{(l)} = GMV_d^{(l)} \hat{\sigma} (GM \hat{\sigma})^{-1} = GMV_d^{(l)} M^{-1} G^{-1} = MG^t V_d^{(l)} (G^t)^{-1} M^{-1}, \tag{2.76}$$

where $GM = MG^t$ is used. Note from (2.33) and (2.34) that $GM = 2\hat{\sigma}V^t = 2V\hat{\sigma}$. Thus the above result is also expressed as

$$A^{(l)} = VV_d^{(l)}V^{-1}, \quad \text{i.e.} \quad \sum_{k=1}^{\infty} A_i^{(l)k} v_j^{(k)} = v_j^{(l)} v_j^{(i)} \quad (\forall i, j, l \in \mathbb{Z}_{\geq 1}). \tag{2.77}$$

This confirms the fact that the effective velocities $v_j^{(l)}$ ($1 \leq j \leq l$) are the eigenvalues of $A^{(l)}$ [15, equation (30)].

We remark that our flux Jacobians form a commuting family:

$$[A^{(l)}, A^{(l')}] = 0 \quad (A^{(1)} = 1). \tag{2.78}$$

This comes from the fact that the matrix V which diagonalizes $A^{(l)}$ does not depend on l (only the eigenvalues depend on l). This property reflects the commutativity $[T_l, T_{l'}] = 0$ of the time evolutions in BBS.

Substitution of (2.71) into the first expression of (2.75) yields

$$A_i^{(l)j} = \sum_{k=1}^{\min(l,i)} \frac{\partial}{\partial \sigma_j} \left(\frac{\sigma_i \sigma_l}{\sigma_{k-1} \sigma_k} \right). \tag{2.79}$$

A little inspection of this shows that $A^{(l)}$ has the block structure whose top left block is of size $l \times l$, the top right one is zero and the bottom right one is $v_l^{(l)}$ times the identity matrix of infinite size:

$$A^{(l)} = \begin{pmatrix} \mathcal{A}^{(l)} & \mathbf{0} \\ \mathcal{U} & v_l^{(l)} \mathbf{I} \end{pmatrix}, \tag{2.80}$$

$$\mathcal{A}^{(l)} = \left(\frac{\partial(\sigma_i v_i^{(l)})}{\partial \sigma_j} \right)_{1 \leq i, j \leq l}, \quad \mathcal{U} = \begin{pmatrix} \sigma_{l+1} u_1 & \sigma_{l+1} u_2 & \dots & \sigma_{l+1} u_l \\ \sigma_{l+2} u_1 & \sigma_{l+2} u_2 & \dots & \sigma_{l+2} u_l \\ \dots & \dots & \dots & \dots \end{pmatrix}, \quad u_j = \frac{\partial v_l^{(l)}}{\partial \sigma_j}. \tag{2.81}$$

For instance $\mathcal{A}^{(3)}$ reads as

$$\mathcal{A}^{(3)} = \begin{pmatrix} 0 & 0 & 1 \\ -\frac{(\sigma_2 + 1)\sigma_3}{\sigma_1^2} & \frac{\sigma_3}{\sigma_1} & \frac{\sigma_2 + 1}{\sigma_1} \\ -\frac{(\sigma_2 + 1)\sigma_3^2}{\sigma_1^2 \sigma_2} & -\frac{\sigma_3(\sigma_1 + \sigma_3)}{\sigma_1 \sigma_2^2} & \frac{\sigma_1 + 2\sigma_2 \sigma_3 + 2\sigma_3}{\sigma_1 \sigma_2} \end{pmatrix}. \tag{2.82}$$

2.6.3. Covariance and Drude matrices. Let us introduce the matrices $C = (C_{i,j})_{i,j \geq 1}$, $B^{(l)} = (B_{i,j}^{(l)})_{i,j \geq 1}$ and $D^{(l)} = (D_{i,j}^{(l)})_{i,j \geq 1}$ whose elements are special cases of $C_{i,j}^{l,m}$ in (2.63):

$$C_{i,j} = C_{i,j}^{1,1} = \sum_p \rho_p \sigma_p (\rho_p + \sigma_p) v_p^{(i)} v_p^{(j)}, \tag{2.83}$$

$$B_{i,j}^{(l)} = C_{i,j}^{1,l} = \sum_p \rho_p \sigma_p (\rho_p + \sigma_p) v_p^{(i)} v_p^{(j)}, \tag{2.84}$$

$$D_{i,j}^{(l)} = C_{i,j}^{l,l} = \sum_p \rho_p \sigma_p (\rho_p + \sigma_p) (v_p^{(i)})^2 v_p^{(j)}. \tag{2.85}$$

The quantities $C_{i,j}^{(l)}$ and $D_{i,j}^{(l)}$ are static covariance and Drude weights [15, equations (158) and (163)].

By using (2.77) it is easy to see

$$A^{(l)} C = C A^{(l)t}, \quad B^{(l)} = A^{(l)} C, \quad D^{(l)} = (A^{(l)})^2 C = A^{(l)} C A^{(l)t}. \tag{2.86}$$

In fact, the first relation is a special case of $\sum_k A_i^{(lk)} \tilde{C}_{k,j} = \sum_k \tilde{C}_{i,k} A_j^{(lk)}$ for $\tilde{C}_{i,j} = \sum_p w_p v_p^{(i)} v_p^{(j)}$ with arbitrary parameters w_k . The equality of the coefficient of each w_p follows directly from (2.77).

Recall the matrix form of the flux Jacobian in (2.76), i.e.,

$$A^{(l)} = M(1 + \hat{y}M)^{-1} V_d^{(l)} (1 + \hat{y}M) M^{-1}. \tag{2.87}$$

Introduce further diagonal matrices

$$\hat{\rho} = \text{diag}(\rho_1, \rho_2, \dots), \quad \hat{g} = 1 + \hat{y} = \text{diag}(1 + y_1, 1 + y_2, \dots). \tag{2.88}$$

Then the formula

$$C_{i,j} = \sum_p \rho_p (1 + y_p) (\sigma_p v_p^{(i)}) (\sigma_p v_p^{(j)}) = \frac{1}{4} \sum_p (GM)_{pi} \rho_p (1 + y_p) (GM)_{pj} \tag{2.89}$$

derived from (2.33) and (2.34) is interpreted as $C = \frac{1}{4} M G^t \hat{\rho} \hat{g} G M$ due to $GM = M G^t$. Applying (2.86) to this and (2.87) we find

$$C = \frac{1}{4} M (1 + \hat{y}M)^{-1} \hat{\rho} \hat{g} (1 + M\hat{y})^{-1} M, \tag{2.90}$$

$$B^{(l)} = \frac{1}{4} M (1 + \hat{y}M)^{-1} V_d^{(l)} \hat{\rho} \hat{g} (1 + M\hat{y})^{-1} M, \tag{2.91}$$

$$D^{(l)} = \frac{1}{4} M (1 + \hat{y}M)^{-1} (V_d^{(l)})^2 \hat{\rho} \hat{g} (1 + M\hat{y})^{-1} M. \tag{2.92}$$

The factor $\frac{1}{4}$ originates in the coefficient 2 in $M_{ij} = 2 \min(i, j)$, which is a non-essential artefact. The results (2.87) and (2.90)–(2.92) agree with [15, equations (165)–(168)].¹¹ We remark a natural generalization

$$C^{(l,m)} := (C_{i,j}^{l,m})_{i,j \geq 1} = A^{(l)} C (A^{(m)})^t (= C^{(m,l)}) \tag{2.93}$$

¹¹ The correspondence with equations (127), (149) and (157) etc in [15] as follows: $\rho_p(k) \leftrightarrow \rho_k$, $\rho_s(k) \leftrightarrow \sigma_k$, $n(k) \leftrightarrow (1 + 1/y_k)^{-1}$, $f(p) \leftrightarrow (1 + y_p)^{-1}$, $E'(p) \leftrightarrow \min(l, p)$ (for T_l BBS dynamics), $h_i(p) \leftrightarrow \min(i, p)$, $(E')^{\text{dr}}(p) \leftrightarrow \sigma_p v_p^{(l)}$, $h_i^{\text{dr}}(p) \leftrightarrow \sigma_p v_p^{(i)}$, $1^{\text{dr}}(p) \leftrightarrow \sigma_p$, $\int \frac{dp}{2\pi} \leftrightarrow \sum_{p=1}^{\infty}$.

Table 3. Drude weight D for a few values of the ball density p and carrier capacity l . For comparison the total current variance f is also given. For $l = 1$ the BBS dynamics reduces to translations. In such a case the spatially integrated current is trivially independent of time and $f = D$ (compare (2.43) and (2.95)).

Ball density p	l	D (2.44) and (2.45)	f (2.95) and (B.7)
p	1	$p(1 - p)$	$p(1 - p)$
0.2	2	0.638 3506	0.672 498
0.2	5	1.744 263	1.857 532
0.2	10	1.901 627	2.023 662
0.4	2	1.606 536	1.790 640
0.4	5	22.570 957	26.048 13
0.4	10	117.6194	134.249 7390

covers $C = C^{(1,1)}, B^{(l)} = C^{(l,1)} = C^{(1,l)}$ and $D^{(l)} = C^{(l,l)}$.

2.7. Equal-time current–current correlations

As a slight digression, we consider here the spatially integrated current

$$J = \sum_x j(x, 0) \tag{2.94}$$

and its variance

$$f = L^{-1} \left(\langle J^2 \rangle - \langle J \rangle^2 \right) = \sum_x \langle j(x, 0) j(0, 0) \rangle^c, \tag{2.95}$$

where the factor L^{-1} insures that f is finite in the thermodynamic limit. The rhs of (2.95) is analogous to the current–current correlation (2.43) which defines the Drude weight, except for the important fact it is an equal-time correlation.

It is possible to compute f using a transfer matrix approach, as explained in appendix B. f of course differs from the Drude weight, but the numerical values turn out to be close (see table 3). Both diverge when approaching the half-filled limit $p \rightarrow 1/2$ at $l = \infty$, and both are equal to $p(1 - p)$ for $l = 1$ (in which case the BBS dynamics reduces to translations). We are however unaware of a simple way to obtain f using TBA. The fact that $f \geq D$ is a general property, which follows from the Cauchy–Schwarz inequality associated to a suitable scalar product between observables (see (3.14) of [37]).

3. Large deviation function

We are interested in the fluctuations of a quantity which, on average, grows linearly with time. In such a case the large deviation function is a useful tool to characterize the fluctuations. In general the large deviation function contains the information about all the cumulants of the fluctuating quantity (full counting statistics)¹². It also describes the rate at which large fluctuations occur [22]. The large deviation function is in general a difficult quantity to obtain, but some important progress has been made recently in the context of integrable systems [28, 29], where a general method to obtain the large deviation function associated to the transport

¹² See however [35, 38] for an example where is this not the case.

of a conserved charge has been constructed. In this section we apply these ideas to the case of the BBS, where the calculations simplify considerably.

3.1. General method

We want to compute the large deviation associated to the number N_t of balls transferred from the left to the right during time t , in some simple GGE stationary state¹³. By definition, if the principle of large deviation is obeyed, we have in the large time limit:

$$F(\lambda) = \lim_{t \rightarrow \infty} \frac{1}{t} \ln [\langle e^{\lambda N_t} \rangle_\beta]. \quad (3.1)$$

Or, in a more compact way:

$$e^{tF(\lambda)} \sim \langle e^{\lambda N_t} \rangle_\beta, \quad (3.2)$$

where $N_t = \sum_{s=0}^t j(0, s)$ is the number of balls passing through the origin during the time interval $[0, t]$. In the above expression the expectation value $\langle f(t) \rangle_\beta$ of an operator f at time t means:

$$\langle f(t) \rangle_\beta = \frac{\sum_c f(c(t)) e^{-\beta Q(c)}}{\sum_c e^{-\beta Q(c)}}, \quad (3.3)$$

where $c(t)$ is the ball configuration c evolved up to time t , and $Q(c)$ is (conserved) total number of balls in c . The parameter β describing the i.i.d. state is related to the ball fugacity by $e^{-\beta} = z$. We focus here on a single conserved quantity (the total number of balls), but the approach can be generalized to a GGE with several β^i coupled to several conserved energies, and a function F of several variables λ^i . See appendix C for a two- β case. Expanding F in powers of λ gives access to the scaled cumulants c_n :

$$F(\lambda) = \sum_{n=1}^{\infty} \frac{\lambda^n}{n!} c_n \quad \text{and} \quad c_n = \lim_{t \rightarrow \infty} \frac{1}{t} \langle (N_t)^n \rangle_\beta^c. \quad (3.4)$$

From the expression above it appears clearly that F is well-defined only if all the cumulants $\langle (N_t)^n \rangle_\beta^c$ have the same t -linear scaling. It should be noted that there are some integrable models where the above relation is not obeyed [38, 39].

Taking the derivative with respect to λ , we have:

$$\frac{dF(\lambda)}{d\lambda} = \lim_{t \rightarrow \infty} \frac{1}{t} \frac{\langle N_t e^{\lambda N_t} \rangle_\beta}{\langle e^{\lambda N_t} \rangle_\beta}, \quad (3.5)$$

where we assume that the above large-time limit exists.

Let us denote by Q_t^L and Q_t^R the charge in the left and right halves of the system at time t . We have $Q_t^L + Q_t^R = Q$, independent of time. Thus,

$$N_t = Q_0^L - Q_t^L = Q - Q_0^R - Q_t^L. \quad (3.6)$$

The relation (3.5) can be written

$$\frac{dF(\lambda)}{d\lambda} = \lim_{t \rightarrow \infty} \frac{1}{t} \frac{\langle N_t e^{-\lambda(Q_0^R + Q_t^L)} \rangle_{\beta-\lambda}}{\langle e^{-\lambda(Q_0^R + Q_t^L)} \rangle_{\beta-\lambda}}, \quad (3.7)$$

¹³ We refer the reader to appendix C for the large deviation function associated to the joint distribution of the number of transferred balls and the number of transferred solitons.

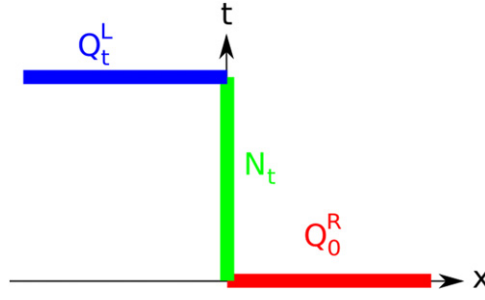


Figure 7. The density operators $n(x > 0, t = 0)$ appearing in Q_0^R are uncorrelated from the current operators $j(x = 0, t > 0)$ in N_t . In the same way, the density operators $n(x < 0, t > 0)$ appearing in Q_t^L are uncorrelated from N_t and from Q_0^R .

where the factor $\exp(\lambda Q)$ has been converted into a shift $\beta \rightarrow \beta - \lambda$.

In the i.i.d. states we consider the equal-time connected correlation of two local operators, $\langle O(x_1, t)O(x_2, t) \rangle^c$ vanish if $x_1 \neq x_2$. But since the ball propagation only takes place in the $x > 0$ direction, we also know, by causality, that a two-time correlation of the form $\langle O(x_1, t_1)O(x_2, t_2) \rangle^c$ vanishes if $(x_1 - x_2)(t_1 - t_2) < 0$. This means that the local terms appearing in $Q_0^R + Q_t^L$ (acting at $x > 0$ and at time 0 or at $x < 0$ and time $t > 0$), and the terms in N_t ($x = 0$ and $t > 0$) are uncorrelated. The term $e^{-\lambda(Q_0^R + Q_t^L)}$ thus decouples from N_t (figure 7) and cancels between the numerator and denominator of (3.7). This leads to

$$\frac{dF(\lambda)}{d\lambda} = \lim_{t \rightarrow \infty} \frac{1}{t} \langle N_t \rangle_{\beta - \lambda}. \tag{3.8}$$

The state defined by $\langle \dots \rangle_{\beta - \lambda}$ is an i.i.d. stationary state, so the expectation value of the currents is independent of time, and we get

$$\frac{dF(\lambda)}{d\lambda} = \langle j(0) \rangle_{\beta - \lambda}, \tag{3.9}$$

where $j(0)$ is the ball current at the origin (and time zero).

The equation (3.9) is closely related to the so-called ‘flow equation’ [28, 29]. As explained in these two works, for a general integrable system the derivative $\frac{dF(\lambda)}{d\lambda}$ of the SCGF is the expectation value $\langle j \rangle_{\tilde{\beta}(\lambda)}$ of the current in a modified GGE state parameterized with modified inverse temperatures $\tilde{\beta}^i(\lambda)$. These inverse temperatures are determined by integrating the flow equation $\frac{d\tilde{\beta}^i}{d\lambda} = -\text{sign}(A(\lambda))_{i^*}^i$ from the initial condition where $\tilde{\beta}^i(0) = \beta^i$ are the parameters of the original GGE (single parameter $e^{-\beta} = z$ in the i.i.d. case we consider). The index i labels the conserved charges and i^* is the index of the particular charge for which the SCGF is computed. We compute here the SCGE associated to the number of balls, so $i^* = \infty$. The matrix $A_{ik}(\lambda) = \partial \langle j_i \rangle_{\tilde{\beta}(\lambda)} / \partial q_k$, is the flux Jacobian (see section 2.6), it appears when linearizing the Euler equations. $A(\lambda)$ is defined by the derivatives of the current densities with respect to the charges densities, evaluated in the λ -modified state. Its eigenvalues are the effective velocities v_i of the normal hydrodynamical modes (the soliton velocities in the BBS case). $\text{sign}(A)$ is defined as the matrix with the same eigenvectors as A but replacing each eigenvalue v_i by $\text{sign}(v_i) = \pm 1$. Here comes a drastic simplification in the BBS case: all the soliton velocities are positive and, therefore, $\text{sign}(A) = \text{Id}$ and the flow equation becomes $\frac{d\tilde{\beta}^i}{d\lambda} = -\delta_{i^*, i}$. Since in the present case $i^* = \infty$ the index i is thus also fixed to $i = \infty$. It follows that the λ -modification

of the state is a simple shift of the parameter β associated to the ball density. The λ -modified state remains i.i.d. but with $\tilde{\beta}(\lambda) = \beta - \lambda$.

3.2. Scaled cumulants generating function

In the rhs of (3.9) we need to consider the mean ball current in a modified i.i.d. state with parameter $\beta' = \beta - \lambda$, and hence a modified ball fugacity $z' = e^{-\beta+\lambda}$.

$$\frac{dF(\lambda)}{d\lambda} = j(e^{-\beta+\lambda}). \tag{3.10}$$

Writing the integration we obtain

$$F(\lambda) = \int_0^\lambda j(e^{-\beta+\lambda'}) d\lambda' = \int_z^{ze^\lambda} \frac{dz'}{z'} j(z'). \tag{3.11}$$

Reintroducing explicitly the parameter l of the dynamics (carrier capacity) and using the explicit form of the ball current (2.9), the integration in (3.11) can be carried out explicitly and gives

$$F^{(l)}(\lambda) = \ln\left(\frac{1 - (ze^\lambda)^{l+1}}{1 - ze^\lambda}\right) - \ln\left(\frac{1 - z^{l+1}}{1 - z}\right). \tag{3.12}$$

As a sanity check we can compute its second derivative at $\lambda = 0$:

$$c_2 = \left. \frac{d^2 F^{(l)}}{d\lambda^2} \right|_{\lambda=0} \tag{3.13}$$

and we recover (2.23).

The appendix C presents some generalization of the above results to a two-temperature GGE, with one parameter coupled to the total number of balls and another one to the total number of solitons. In particular a generalization of (3.12) is given in (C.23).

It is useful to consider the Legendre transform of F with respect to λ , the so-called large-deviation rate function:

$$G(j) = j\lambda(j) - F(\lambda(j)), \tag{3.14}$$

where $\lambda(j)$ is a solution of

$$F'(\lambda(j)) = j. \tag{3.15}$$

The probability to observe a transferred charge $N = jt$ at time t is then

$$P_t(N) \sim \exp(-t G(N/t)). \tag{3.16}$$

$G(j)$ is defined for $0 < j < l$, since the maximum possible value of the ball current is l . It is a convex function obeying $G(0) = \ln((1 - z^{l+1})/(1 - z))$, $G(l) = G(0) - l \ln(z)$ reaching its maximum zero at the mean current $j = F'(0)$. The function G is represented in figure 8, in the vicinity of its maximum, for one particular case ($p = z/(1 + z) = 0.3$ and $l = 10$).

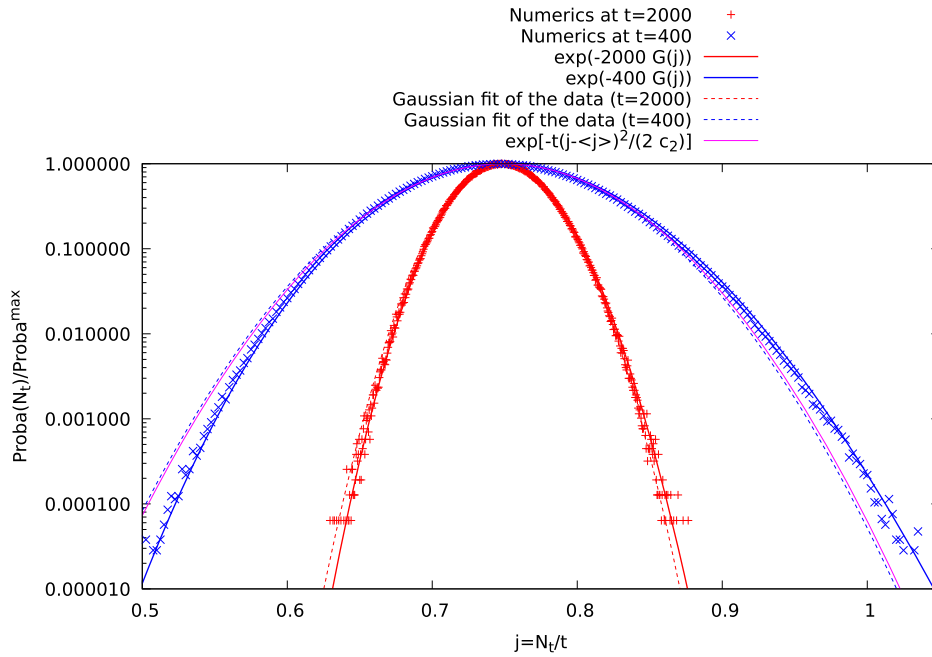


Figure 8. Probability distribution of the number N_t of balls having crossed the origin between $t = 0$ and $t = 400$ (blue), and between $t = 0$ and $t = 2000$ (red). Ball density $p = 0.3$ and capacity $l = 10$. The numerical data at $t = 400$ are obtained using 6×10^6 random initial conditions and the data at $t = 2000$ involve 2×10^6 random initial conditions. These results are compared with the Gaussian obtained by doing a least-square fit of the data (dashed lines). Such a fit has two free parameters: mean and variance. The data at $t = 400$ are also compared to the Gaussian $\exp[-t(j - \langle j \rangle)^2 / (2c_2)]$ (magenta line), without any adjustable parameter, where $\langle j \rangle = 0.7490144$ is the exact mean value of the current (2.9) and $c_2 = 1.3016578$ is the exact second cumulant (2.23). Finally, the data are compared to the exact large deviation rate function (continuous lines) $\exp(-tG(N/t))$. At $t = 400$ it is possible to see that the numerical data departs from a simple Gaussian and are instead consistent with the theoretical prediction involving the large deviation rate function G (3.14).

3.3. $l = \infty$

In the limit $l \rightarrow \infty$ the SCGF (3.12) simplifies to

$$F^{(\infty)}(\lambda) = \ln \left(\frac{1 - z}{1 - ze^\lambda} \right). \tag{3.17}$$

The interval where F is defined is $\lambda \in [-\infty, \beta]$, which is equivalent to $ze^\lambda < 1$ (recall that $z = e^{-\beta}$). For $\lambda \rightarrow -\infty$ the current $j = F'(\lambda)$ tends to zero, and for $\lambda \rightarrow \beta$ we have instead $j = F'(\lambda) \rightarrow +\infty$. The full range of physical values for the ball current is covered by F' , as it should. A generalization of (3.17) to a two-temperature GGE is given in (C.26).

In that case the large-deviation rate function can be obtained explicitly:

$$G^{(\infty)}(j) = -\ln(1 - z) - j \ln(z) - (1 + j) \ln(1 + j) + j \ln(j). \tag{3.18}$$

This function is plotted in figure 9 for a few different values of the ball fugacity. The generalization to a two-temperature GGE is given in (C.28). When $z \rightarrow 1^-$ $F^{(\infty)}(\lambda)$ becomes singular

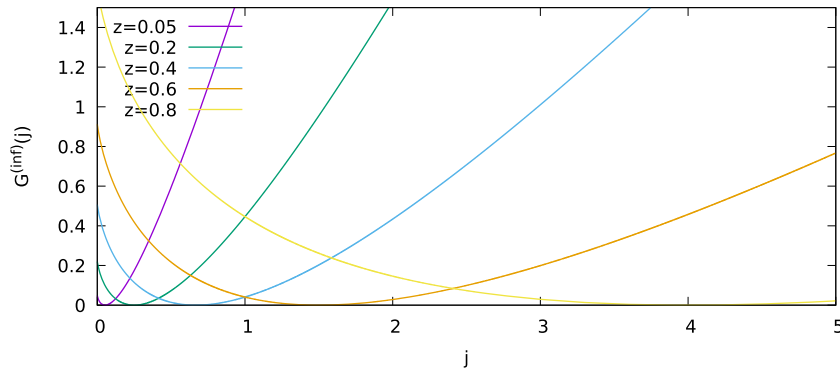


Figure 9. Large-deviation rate function $G^{(l=\infty)}(j)$ plotted as a function of the current j , for different values of the ball fugacity z . The mean current (minimum of G) and the second cumulant c_2 diverge when $z \rightarrow 1^-$.

in $\lambda = 0$ and the associated cumulants diverge. For instance: $c_2 = z/(1 - z)^2$ at $l = \infty$. This can be interpreted as a phase transition when the ball density approaches $1/2$. Some other properties of this transition were discussed in [3].

To conclude this section we note that the large deviation principle for the energies E_k in i.i.d. states was studied for a multicolor BBS by regarding the history of carriers going through the states as a Markov process [11]. In that previous study the system size is the variable which plays a role similar to the role played by time here.

4. Conclusions

We have computed analytically several quantities related to the current and density fluctuations in stationary i.i.d. states. We have obtained the SCGF associated to the number N_t of balls crossing the origin during time t , from which all the cumulants can be extracted. The Legendre transform of this function could be compared with the probability distribution of N_t extracted from numerical simulations. This is one of the very few interacting and deterministic models where the SCGF could be computed exactly ([38] is another recent example).

The Drude weights—defined as the long-time limit of a spatially integrated current–current correlation—could also be obtained using TBA combined with hydrodynamical projection. Explicit analytical expressions for the Drude weights could be compared successfully with numerical simulations.

The existence of a family of commuting time evolutions is an important property of integrable systems, although implementing them in actual systems can be cumbersome in practice. The BBS is a distinguished example of integrable cellular automata where the all commuting time evolutions have a simple and neat implementation. Exploiting these time evolutions a set of new generalized currents correlations (or generalized Drude weights) was constructed and shown to enjoy unexpected symmetry relations. Some of these symmetry relations can be explained at the microscopic level, while others only emerge in the long-time limit. We observed that the numerical results for the current correlations at long times coincide with the TBA results only for certain time evolution, namely T_n with sufficiently large n . This suggests that T_n for small n is insufficiently mixing and the observed correlations in this regime still escape our understanding. Understanding these results and reconciling them with the hydrodynamic projection ideas would certainly deserve further study.

We also stress that a number of these results could be generalized to a larger family of (non i.i.d.) GGE states with two temperatures, respectively coupled to the number of balls and to the number of solitons.

It is quite remarkable that so many explicit formulae could be obtained for nontrivial quantities related to long-distance and long-time limit of correlations in such an out-of-equilibrium interacting problem. These could prove to be useful to compare BBS with other models, either integrable or non-integrable, and to shed some light about fundamental questions like the emergence of hydrodynamics.

Acknowledgments

VP thanks E Ilievski, Z Krajnik, T Prosen and J Schmidt for numerous discussions and collaboration on related subjects. We also acknowledge the DRF of CEA for providing us with CPU time on the supercomputer TOPAZE at CCRT.

Data availability statement

The data that support the findings of this study are available upon reasonable request from the authors.

Appendix A. Correlation sum rules

We derive a sum rule connecting density–density correlations to current–current ones. The argument is directly inspired from [30]. We consider the following quantity

$$\sum_{x=-\infty}^{\infty} f(x) (n(x, t) - n(x, 0)), \tag{A.1}$$

where n is the ball density operator, and f some test function defined on the lattice sites. Next we introduce the charge of the region $] - \infty, x]$:

$$N^{\leftarrow}(x, t) = \sum_{y=-\infty}^x n(y, t) \tag{A.2}$$

$$n(x, t) = N^{\leftarrow}(x, t) - N^{\leftarrow}(x - 1, t) \tag{A.3}$$

(A.1) can be rewritten as

$$\sum_{x=-\infty}^{\infty} f(x) (n(x, t) - n(x, 0)) = \sum_{x=-\infty}^{\infty} f(x) \left(N^{\leftarrow}(x, t) - N^{\leftarrow}(x - 1, t) - N^{\leftarrow}(x, 0) + N^{\leftarrow}(x - 1, 0) \right) \tag{A.4}$$

$$= \sum_{x=-\infty}^{\infty} (f(x) - f(x + 1)) \left(N^{\leftarrow}(x, t) - N^{\leftarrow}(x, 0) \right) \tag{A.5}$$

$$= - \sum_{x=-\infty}^{\infty} (f(x) - f(x + 1)) \int_0^t j(x + 1, s) ds \tag{A.6}$$

$$= \sum_{x=-\infty}^{\infty} (f(x) - f(x - 1)) \int_0^t j(x, s) ds. \tag{A.7}$$

The current can also be used to write

$$n(0, t) - n(0, 0) = \int_0^t (j(0, s) - j(1, s)) ds. \tag{A.8}$$

We then multiply (A.7) by (A.8)

$$\begin{aligned} & \sum_{x=-\infty}^{\infty} f(x) (n(x, t) - n(x, 0)) (n(0, t) - n(0, 0)) \\ &= \sum_{x=-\infty}^{\infty} (f(x) - f(x - 1)) \int_0^t j(x, s) ds \int_0^t (j(0, s') - j(1, s')) ds' \end{aligned} \tag{A.9}$$

and take the connected average:

$$\begin{aligned} & \sum_{x=-\infty}^{\infty} f(x) \langle (n(x, t) - n(x, 0)) (n(0, t) - n(0, 0)) \rangle^c \\ &= \sum_{x=-\infty}^{\infty} \int_0^t \int_0^t ds ds' (f(x) - f(x - 1)) \langle j(x, s) (j(0, s') - j(1, s')) \rangle^c \end{aligned} \tag{A.10}$$

$$= \sum_{x=-\infty}^{\infty} \int_0^t \int_0^t ds ds' (f(x) - f(x - 1)) \langle (j(x, s) - j(x - 1, s)) j(0, s') \rangle^c, \tag{A.11}$$

where, in the last equality, we have used the translation invariance of the current–current correlator. This can finally be rewritten

$$\begin{aligned} & \sum_{x=-\infty}^{\infty} f(x) \langle (n(x, t) - n(x, 0)) (n(0, t) - n(0, 0)) \rangle^c \\ &= \sum_{x=-\infty}^{\infty} \int_0^t \int_0^t ds ds' (2f(x) - f(x + 1) - f(x - 1)) \langle j(x, s) j(0, s') \rangle^c. \end{aligned} \tag{A.12}$$

Appendix B. Transfer matrix calculation for the current fluctuations

This section presents a transfer matrix calculation of the fluctuations of the current (2.95). It is an extension of the calculation presented in the appendix E of [12].

Here we consider the periodic BBS model on a chain of length L . It admits a discrete set of commuting evolutions characterized by a row to row transfer propagator T_l labelled by a positive integer l representing the capacity of the carrier. The propagator T_l takes the form of a vertex transfer matrix (see figure B1) where the horizontal links can contain up to l balls which are auxiliary variables: $0 \leq n^c \leq l$. The vertical links contain zero or one ball: $0 \leq n^b \leq 1$ which are the BBS variables. Time flows down, so that at each time step, the south vertical

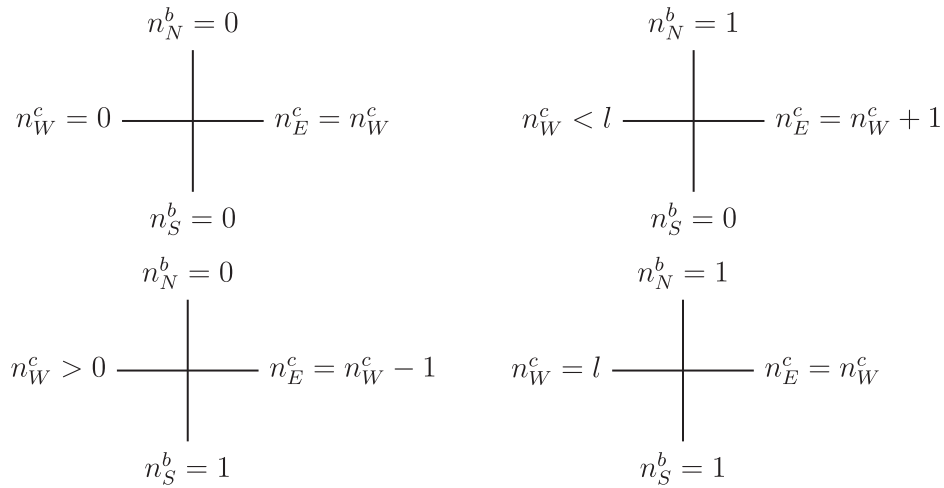


Figure B1. Four examples of vertices.

links are occupied according to the north vertical link configurations. We can see the evolution as the result of the passage of a carrier transporting up to l balls from west to east and updating each vertical link successively passing through the vertices. If the north vertical link is empty ($n_N^b = 0$) and the carrier has at least one ball ($n_W^c > 0$), it leaves one of its balls to the south vertical link during the passage ($n_S^b = 1, n_E^c = n_W^c - 1$). If it does not carry balls ($n_W^c = 0$), it passes without changing either the vertical occupation or its load ($n_S = 0, n_E^c = 0$). If the north vertical link is filled ($n_N^b = 1$) and the carrier carries strictly less than l balls ($n_W^c < l$), it picks up a ball and leaves the south vertical link empty ($n_E^c = n_W^c + 1, n_S^b = 0$). If it carries l balls ($n_W^c = l$), it passes without changing either the vertical occupation or its load ($n_S^b = 1, n_E^c = l$). On a periodic chain, it can be shown (proposition 5.1 of [2]) that the periodicity condition on the horizontal links uniquely determines the load of the carrier¹⁴.

As a result, the transfer propagator can be expressed as:

$$(T_l)_{n^b(t+1)}^{n^b(t)} = \langle n^b(t+1) | \text{Tr} \left(\prod_{k=1}^L \mathbb{L}_k \right) | n^b(t) \rangle, \tag{B.1}$$

where $n_b(t)$ stands for the configuration $\{n^b(x, t), 1 \leq x \leq L\}$ and $\langle n_S^b | \mathbb{L} | n_N^b \rangle = \langle n_S^b | \mathbb{L} | n_N^b \rangle_{n_W^c, n_E^c}$ is a $(l+1) \times (l+1)$ permutation matrix with nonzero matrix elements equal to one whenever the corresponding vertex is allowed.

Due to charge conservation, $n_N + n_W = n_S + n_E$, the ball density $n^b(x, t)$ coincides with the number of balls on the vertical links and the ball current $j(x, t) = n^c(x, t)$ to the number of balls on the horizontal links.

We can give a fugacity to the balls by inserting the operator $z^Q = z^{\sum_{x=1}^L n^b(x, t)}$ which commutes with the propagator. Denote $|0\rangle$ the state obtained by summing all the ball configurations with weight one. The i.i.d. stationary state with ball density $p = z/(z+1)$ is $z^Q|0\rangle$.

We can also give a fugacity to the total current at time t by weighting the horizontal links by $y^{j(t)} = y^{\sum_{x=1}^L j(x, t)}$. We denote by $T_l(y)$ (or $\mathbb{L}(y)$ for a single site) the modified propagator where

¹⁴ To be precise: it is so when the density is not exactly equal to $1/2$.

we weight each vertex by y^{n^c} instead of 1, which has the effect to weight each configuration by $y^{J(t)}$.

$$\mathbb{L}^a(y)_{i,j} = \begin{cases} y^i & \text{if } i \begin{array}{c} \text{---} a \\ | \\ \text{---} a^* \end{array} j \text{ is in Figure B1 } (a^* = a + i - j) \\ 0 & \text{otherwise.} \end{cases} \quad (\text{B.2})$$

Consider the matrix element $Z = \langle 0 | z^Q y^{J(t)} | 0 \rangle = \text{Tr}(\mathbb{L}^0(y) + z\mathbb{L}^1(y))^L$ where $\mathbb{L}^0(y), \mathbb{L}^1(y)$ are the deformed vertex matrices with $n_N^0 = 0, 1$ respectively (n_S^0 is redundant).

Denoting $\mathbb{L}^z(y) = \mathbb{L}^0(y) + z\mathbb{L}^1(y)$, we have:

$$\begin{aligned} \langle 0 | \mathbb{L}^z(y) &= \langle 0 | + z \langle 1 | \\ \langle n | \mathbb{L}^z(y) &= y^n \langle n-1 | + zy^n \langle n+1 | \quad \text{if } n \neq 0, l \\ \langle l | \mathbb{L}^z(y) &= y^l \langle l-1 | + zy^l \langle l |. \end{aligned} \quad (\text{B.3})$$

As an example, for $l = 3$ we have

$$\mathbb{L}^z(y) = \begin{pmatrix} 1 & z & 0 & 0 \\ y & 0 & zy & 0 \\ 0 & y^2 & 0 & zy^2 \\ 0 & 0 & y^3 & zy^3 \end{pmatrix}. \quad (\text{B.4})$$

The matrix element $\mathbb{L}^z(1)_{\alpha,\beta}/(z+1)$ is the probability to have β balls on the east link knowing that there are α on the west link. Therefore, the components of the left eigenvector of $\mathbb{L}^z(1)/(z+1)$ with eigenvalue one, $\sum_{k=0}^l z^k \langle k |$, are the unnormalized probabilities for the carrier to contain k balls. The current formula (2.9) is obtained as the average number of balls in the carrier.

The second cumulant c_2 and f , the integrated current–current connected correlation, are then given by second derivatives of $\ln(Z)$:

$$c_2 = \frac{1}{L} \left(z \frac{\partial}{\partial z} \right) \left(y \frac{\partial}{\partial y} \right) \ln(Z)|_{y=1}, \quad (\text{B.5})$$

$$f = \langle J(0)j(0,0) \rangle^c = \frac{1}{L} \left(y \frac{\partial}{\partial y} \right)^2 \ln(Z)|_{y=1}. \quad (\text{B.6})$$

By analyzing the values of f for various values of l , it has also been possible to conjecture the following analytical expression for f :

$$\begin{aligned} f = & \frac{z(1+6z+z^2)(1-z^{3l+3})}{(1-z)^4(1-z^{l+1})^3} - \frac{24z^{l+5}(1-z^{l-3})}{(1-z)^4(1-z^{l+1})^3} \\ & - \frac{3z^{l+2}(g_{l+2}+7zg_l+8z^2g_{l-2})}{(1-z)^3(1-z^{l+1})^3} - \frac{(l+1)^2z^{l+1}(g_{l+2}+2l(1+z)g_{l+1}+3zg_l)}{(1-z)(1-z^{l+1})^3}, \end{aligned} \quad (\text{B.7})$$

where $g_j = 1 + z^j$.

Appendix C. Drude weight and SCGF in a two-temperature GGE

The BBS has the conserved quantities $E_k = L \sum_{j \geq 1} \min(j, k) \rho_j$ for $k = 1, 2, \dots$ [12]. E_∞ is the total number of balls with which the main text is concerned. In this appendix we present a partial generalization of the results to the two-temperature GGE corresponding to the statistical weight $e^{-\beta_1 E_1 - \beta_\infty E_\infty}$. The conserved quantity E_1 is the number of solitons. The inverse temperature β in the main text is denoted by β_∞ here.

Following [12] (3.20) we parameterize the temperatures by a, z as

$$e^{\frac{1}{2}\beta_1} = \frac{a^{\frac{1}{2}} - a^{-\frac{1}{2}}}{z^{\frac{1}{2}} - z^{-\frac{1}{2}}}, \quad e^{-\beta_\infty} = z. \tag{C.1}$$

The single temperature GGE(β_∞) corresponds to the limit $a \rightarrow z$. Derivatives by the temperatures are expressed in terms of a and z as in equations (3.22) and (3.23) in [12]:

$$\frac{\partial}{\partial \beta_1} = \frac{\partial a}{\partial \beta_1} \frac{\partial}{\partial a} + \frac{\partial z}{\partial \beta_1} \frac{\partial}{\partial z} = -\frac{a(1-a)}{1+a} \frac{\partial}{\partial a}, \tag{C.2}$$

$$\frac{\partial}{\partial \beta_\infty} = \frac{\partial a}{\partial \beta_\infty} \frac{\partial}{\partial a} + \frac{\partial z}{\partial \beta_\infty} \frac{\partial}{\partial z} = -\frac{a(1-a)(1+z)}{(1+a)(1-z)} \frac{\partial}{\partial a} - z \frac{\partial}{\partial z}. \tag{C.3}$$

Densities, effective velocity and currents have been obtained in [12] as follows ((C.7) was not included therein):

$$\sigma_k = \frac{(1-a)(1+az^k)}{(1+a)(1-az^k)}, \quad \rho_k = \frac{az^{k-1}(1-a)(1-z)^2(1+az^k)}{(1+a)(1-az^{k-1})(1-az^k)(1-az^{k+1})}, \tag{C.4}$$

$$v_k^{(l)} = \frac{1+az^l}{1-az^l} v_{\min(k,l)}, \quad v_k = \frac{1+a}{1-a} k - \frac{2a(1+z)(1-z^k)}{(1-a)(1-z)(1+az^k)}. \tag{C.5}$$

$$\text{ball current: } j_\infty^{(l)} = \sum_{k \geq 1} k \rho_k v_k^{(l)} = \frac{a(1+z)(1-z^l)}{(1+a)(1-z)(1-az^l)} - \frac{laz^l}{1-az^l}, \tag{C.6}$$

$$\text{soliton current: } j_1^{(l)} = \sum_{k \geq 1} \rho_k v_k^{(l)} = \frac{a(1-z^l)}{(1+a)(1-az^l)}. \tag{C.7}$$

The results (C.6) and (C.7) are the $j = \infty$ and $j = 1$ cases of (2.57):

$$\eta_j^{(l)} = \frac{a(1+z)(1-z^{\min(j,l)})(1+az^{\max(j,l)})}{(1+a)(1-z)(1-az^j)(1-az^l)} - \frac{\min(j,l)a(z^j+z^l)}{(1-az^j)(1-az^l)}. \tag{C.8}$$

Set $W_i = \rho_i \sigma_i (\rho_i + \sigma_i) v_i^2$ as in the main text. Then the sum formula (2.51) admits the following generalization:

$$\sum_{i < l} W_i = \frac{a(1-a)(1+z)A_l}{(1+a)^3(1-z)(1-az^{l-1})^2(1-az^l)^2}, \tag{C.9}$$

$$A_l = 1 + 2a(1+a^2)z^{2l-1} + a^4z^{4l-2} + a^2z^{2l-2}(1+8z+z^2) - az^{l-1}(2+a^3z^{2l-1})g_l(z) - z^l(1+2a^3z^{2l-1})g_l(z^{-1}) - a^2z^{l-1}h_l(z) - a^2z^{3l-1}h_l(z^{-1}), \tag{C.10}$$

$$\begin{aligned}
 g_l(z) &= \frac{z + (1 - l(1 - z))^2}{1 + z}, \\
 h_l(z) &= (1 + l)^2 + l^2 z + \frac{(1 - 2l + z)(3 + z + 2lz)}{1 + z}.
 \end{aligned}
 \tag{C.11}$$

This is easily shown by induction on l and $A_0 = A_1 = 0$. The above A_l precisely reduces to (2.51) in the single temperature case $a = z$.

Define the second cumulant $c_2^{(l)}$ and the Drude weight $D^{(l)}$ by (2.41) and (2.45) with $\rho_i, \sigma_i, v_i^{(l)}$ specified in (C.4) and (C.5). From $v_i^{(1)} = 1$ we have

$$D^{(1)} = \sum_{i \geq 1} W_i = \frac{a(1 - a)(1 + z)A_\infty}{(1 + a)^3(1 - z)} = \frac{a(1 - a)(1 + z)}{(1 + a)^3(1 - z)},
 \tag{C.12}$$

$$\begin{aligned}
 c_2^{(l)} &= \frac{a(1 - a)(1 + z)^2(1 - z^l)(1 + a^2 z^l)}{(1 + a)^3(1 - z)^2(1 - az^l)^2} + \frac{2az(1 - z^l)}{(1 + a)(1 - z)^2(1 - az^l)} \\
 &\quad - \frac{alz^l}{(1 - az^l)^2} \left(l + \frac{2(1 - a)(1 + z)}{(1 + a)(1 - z)} \right)
 \end{aligned}
 \tag{C.13}$$

$$= -\frac{\partial j_\infty^{(l)}}{\partial \beta_\infty}.
 \tag{C.14}$$

For $D^{(l)}$ with general l , formally the same formula as (2.54) with $\frac{z}{(1+z)^2}$ replaced by (C.12) is valid. These results reduce to the single temperature case at $a = z$. Another useful sum formula is

$$\sum_{i \geq r} \rho_i \sigma_i (\rho_i + \sigma_i) = \frac{a(1 - a)^3(1 - z)z^{r-1} (1 + a^2 z^{2r-1})}{(1 + a)^3(1 - az^{r-1})^2(1 - az^r)^2}.
 \tag{C.15}$$

The ball density p in the two-temperature GGE is known to be $p = \frac{a}{1+a}$ in [12, (3.23)]. Unlike (2.46), the result (C.12) does not coincide with the $p(1 - p)$ reflecting the fact that the two-temperature GGE under consideration is *not* i.i.d.

It is natural to introduce the joint cumulant generating function

$$F(\lambda, \mu) = \lim_{t \rightarrow \infty} \frac{1}{t} \ln \langle e^{\lambda N_{\infty,t} + \mu N_{1,t}} \rangle_{\beta_\infty, \beta_1},
 \tag{C.16}$$

where the superscript l is suppressed and $N_{\infty,t} = \int_0^t j_\infty^{(l)}(0, \tau) d\tau$ and $N_{1,t} = \int_0^t j_1^{(l)}(0, \tau) d\tau$. By the same argument as before, we have

$$\frac{\partial F(\lambda, \mu)}{\partial \lambda} = j_\infty^{(l)}(\beta_\infty - \lambda, \beta_1 - \mu), \quad \frac{\partial F(\lambda, \mu)}{\partial \mu} = j_1^{(l)}(\beta_\infty - \lambda, \beta_1 - \mu).
 \tag{C.17}$$

Let (ζ, α) be the parameters (z, a) corresponding to $(\beta_\infty - \lambda, \beta_1 - \mu)$ in the sense of (C.1). Then from (C.6) and (C.7) the currents are expressed as

$$j_\infty^{(l)}(\beta_\infty - \lambda, \beta_1 - \mu) = \frac{\alpha(1 + \zeta)(1 - \zeta^l)}{(1 + \alpha)(1 - \zeta)(1 - \alpha\zeta^l)} - \frac{l\alpha\zeta^l}{1 - \alpha\zeta^l},
 \tag{C.18}$$

$$j_1^{(l)}(\beta_\infty - \lambda, \beta_1 - \mu) = \frac{\alpha(1 - \zeta^l)}{(1 + \alpha)(1 - \alpha\zeta^l)}.
 \tag{C.19}$$

Here (ζ, α) are regarded as functions of (λ, μ) including (z, a) as parameters. Namely,

$$\frac{\alpha^{\frac{1}{2}} - \alpha^{-\frac{1}{2}}}{\zeta^{\frac{1}{2}} - \zeta^{-\frac{1}{2}}} = e^{\frac{1}{2}(\beta_1 - \mu)} = \frac{a^{\frac{1}{2}} - a^{-\frac{1}{2}}}{z^{\frac{1}{2}} - z^{-\frac{1}{2}}} e^{-\frac{1}{2}\mu} \quad \zeta = e^{-\beta_\infty + \lambda} = ze^\lambda. \quad (\text{C.20})$$

They imply the derivative relations similar to (C.2) and (C.3):

$$\frac{\partial}{\partial \lambda} = \frac{\alpha(1 - \alpha)(1 + \zeta)}{(1 + \alpha)(1 - \zeta)} \frac{\partial}{\partial \alpha} + \zeta \frac{\partial}{\partial \zeta}, \quad \frac{\partial}{\partial \mu} = \frac{\alpha(1 - \alpha)}{1 + \alpha} \frac{\partial}{\partial \alpha}. \quad (\text{C.21})$$

By using (C.18), (C.19) and (C.21), one can directly check the consistency of (C.17):

$$\frac{\partial J_\infty^{(l)}(\beta_\infty - \lambda, \beta_1 - \mu)}{\partial \mu} = \frac{\partial J_1^{(l)}(\beta_\infty - \lambda, \beta_1 - \mu)}{\partial \lambda}. \quad (\text{C.22})$$

The solution to (C.17) satisfying $F(0, 0) = 0$ is given by

$$F(\lambda, \mu) = \ln \left(\frac{1 - \alpha \zeta^l}{1 - \alpha} \right) - \ln \left(\frac{1 - az^l}{1 - a} \right), \quad (\text{C.23})$$

where $\alpha = \alpha(\lambda, \mu)$ and $\zeta = \zeta(\lambda, \mu) (= ze^\lambda)$ are specified as the solution to (C.20) satisfying $\alpha > 0$. Note that $\alpha(\lambda, \mu = 0)|_{a=z} = ze^\lambda$. Thus, the result (C.23) provides a generalization of (3.12) reproducing the latter as $F(\lambda, \mu = 0)|_{a=z} = F^{(l)}(\lambda)$.

One can check $\left. \frac{\partial^2 F}{\partial \lambda^2} \right|_{\lambda=\mu=0} = c_2^{(l)}$. The other second order scaled cumulants are given by

$$\begin{aligned} \lim_{t \rightarrow \infty} \frac{1}{t} \langle N_{\infty, t} N_{1, t} \rangle_{\beta_\infty, \beta_1}^c &= \left. \frac{\partial^2 F}{\partial \lambda \partial \mu} \right|_{\lambda=\mu=0} \\ &= \frac{a(1-a) \left((1+z)(1-z^l)(1+a^2z^l) - (1+a)^2(1-z)lz^l \right)}{(1+a)^3(1-z)(1-az^l)^2}, \end{aligned} \quad (\text{C.24})$$

$$\lim_{t \rightarrow \infty} \frac{1}{t} \langle N_{1, t}^2 \rangle_{\beta_\infty, \beta_1}^c = \left. \frac{\partial^2 F}{\partial \mu^2} \right|_{\lambda=\mu=0} = \frac{a(1-a)(1-z^l)(1+a^2z^l)}{(1+a)^3(1-az^l)^2}. \quad (\text{C.25})$$

We leave an interesting problem of studying the Hessian of F in relation to the convexity of F for a future work.

When $l = \infty$, (C.23) in the regime $ze^\lambda < 1$ simplifies to

$$F^{(\infty)}(\lambda, \mu) = \ln \left(\frac{1-a}{1-\alpha} \right). \quad (\text{C.26})$$

This is still a non-trivial function of λ and μ via (C.20). From (C.17)–(C.19) with $l = \infty$, the equation $\left(\frac{\partial F^{(\infty)}(\lambda, \mu)}{\partial \lambda}, \frac{\partial F^{(\infty)}(\lambda, \mu)}{\partial \mu} \right) = (\mathcal{J}_\infty, \mathcal{J}_1)$ has the solution

$$\lambda_* = \ln \left(\frac{\mathcal{J}_\infty - \mathcal{J}_1}{z(\mathcal{J}_\infty + \mathcal{J}_1)} \right), \quad \mu_* = \ln \left(\frac{4(1 - \mathcal{J}_1)\mathcal{J}_1^3(a + a^{-1} - 2)}{(\mathcal{J}_\infty^2 - \mathcal{J}_1^2)(1 - 2\mathcal{J}_1)^2(z + z^{-1} - 2)} \right), \quad (\text{C.27})$$

which is deduced from $\alpha_* = \frac{\mathcal{J}_1}{1-\mathcal{J}_1}$, $\zeta_* = \frac{\mathcal{J}_\infty - \mathcal{J}_1}{\mathcal{J}_\infty + \mathcal{J}_1}$. Now the large deviation rate function $G^{(\infty)}(\mathcal{J}_\infty, \mathcal{J}_1) = \mathcal{J}_\infty \lambda_* + \mathcal{J}_1 \mu_* - F^{(\infty)}(\lambda_*, \mu_*)$ is given by

$$\begin{aligned}
 G^{(\infty)}(\mathcal{J}_\infty, \mathcal{J}_1) &= \mathcal{J}_\infty \ln \left(\frac{\mathcal{J}_\infty - \mathcal{J}_1}{z(\mathcal{J}_\infty + \mathcal{J}_1)} \right) \\
 &+ \mathcal{J}_1 \ln \left(\frac{4(1 - \mathcal{J}_1)\mathcal{J}_1^3(a + a^{-1} - 2)}{(\mathcal{J}_\infty^2 - \mathcal{J}_1^2)(1 - 2\mathcal{J}_1)^2(z + z^{-1} - 2)} \right) \\
 &- \ln \left(\frac{(1 - a)(1 - \mathcal{J}_1)}{1 - 2\mathcal{J}_1} \right).
 \end{aligned} \tag{C.28}$$

Since every soliton carries at least one ball, the ball current \mathcal{J}_∞ and the soliton current \mathcal{J}_1 are to be considered in the domain $\mathcal{J}_\infty > \mathcal{J}_1$. Similarly, from (C.7) with $l \rightarrow \infty$, one should suppose $\mathcal{J}_1 < 1$. Note that $G^{(\infty)}(\mathcal{J}_\infty, \mathcal{J}_1)$ is finite at $\mathcal{J}_1 = \frac{1}{2}$.

The single temperature case in the main text corresponds to setting $a = z$, $\mu = 0$. In fact, (C.20) enforces $\alpha_* = \zeta_*$ leading to $\mathcal{J}_1 = \frac{\mathcal{J}_\infty}{1+2\mathcal{J}_\infty}$ and $\mu_* = 0$. Then (C.28) reduces $G^{(\infty)}(j = \mathcal{J}_\infty)$ in the main text.

Appendix D. Microscopic definition of $\hat{\eta}_i^{(l)}(\mathbf{x})$

Here we outline the proof of the properties of the generalized current $\hat{\eta}_i^{(l)}(x)$ claimed in the beginning of section 2.4. We begin by recalling the combinatorial R in the crystal base theory, a theory of quantum groups at $q = 0$, for which readers are referred to [2, section 2.2] and the references therein.

For a positive integer l , define a set $B_l = \{\alpha = (\alpha_0, \alpha_1) \in (\mathbb{Z}_{\geq 0})^2 \mid \alpha_0 + \alpha_1 = l\}$. Introduce an infinite set known as an affine crystal $\text{Aff}(B_l) = B_l \times \zeta^{\mathbb{Z}} = \{\alpha \zeta^n \mid \alpha \in B_l, n \in \mathbb{Z}\}$, where ζ is an indeterminate. Define a map $R_{l,m} : \text{Aff}(B_l) \otimes \text{Aff}(B_m) \rightarrow \text{Aff}(B_m) \otimes \text{Aff}(B_l)$ by¹⁵

$$R_{l,m} : \alpha \zeta^a \otimes \beta \zeta^b \mapsto \tilde{\beta} \zeta^{b+H(\alpha \otimes \beta)} \otimes \tilde{\alpha} \zeta^{a-H(\alpha \otimes \beta)} \tag{D.1}$$

for any $a, b \in \mathbb{Z}$. Here for $\alpha = (\alpha_0, \alpha_1) \in B_l, \beta = (\beta_0, \beta_1) \in B_m$, the image $\tilde{\alpha} = (\tilde{\alpha}_0, \tilde{\alpha}_1) \in B_l, \tilde{\beta} = (\tilde{\beta}_0, \tilde{\beta}_1) \in B_m$ and $H(\alpha \otimes \beta) \in \mathbb{Z}$ are specified by

$$\begin{aligned}
 \tilde{\alpha}_i &= \alpha_i + \min(\alpha_{i+1}, \beta_i) - \min(\alpha_i, \beta_{i+1}), \\
 \tilde{\beta}_i &= \beta_i - \min(\alpha_{i+1}, \beta_i) + \min(\alpha_i, \beta_{i+1}),
 \end{aligned} \tag{D.2}$$

$$H(\alpha \otimes \beta) = \min(\alpha_0, \beta_1) \tag{D.3}$$

with all the indices in \mathbb{Z}_2 . The map $R_{l,m}$ is called an (affine) combinatorial R . It is the quantum R matrix for (spin $l/2$ rep) \otimes (spin $m/2$ rep) of $U_q(\widehat{sl}_2)$ at $q = 0$ with respect to the crystal base, which retains all the combinatorial essence. The indeterminate ζ is a remnant of the spectral parameter of the R matrices. The simpler version forgetting it (the one formally corresponding to $\zeta = 1$) is called (classical) combinatorial R . In what follows the both versions will simply

¹⁵ Tensor product \otimes in this appendix can just be regarded as product of sets.

be denoted by R . The relation (D.1) is customarily depicted as

$$\begin{array}{ccc}
 & \beta\zeta^b & \\
 & \downarrow & \\
 \alpha\zeta^a & \xrightarrow{\quad} & \tilde{\alpha}\zeta^{a-H} \\
 & \downarrow & \\
 & \tilde{\beta}\zeta^{b+H} &
 \end{array}
 \quad (H = H(\alpha \otimes \beta)).$$

It satisfies the inversion and the Yang–Baxter relations

$$R_{m,l}R_{l,m} = \text{Id}, \tag{D.4}$$

$$(1 \otimes R_{k,l})(R_{k,m} \otimes 1)(1 \otimes R_{l,m}) = (R_{l,m} \otimes 1)(1 \otimes R_{k,m})(R_{k,l} \otimes 1), \tag{D.5}$$

which are equalities of the maps $\text{Aff}(B_l) \otimes \text{Aff}(B_m) \rightarrow \text{Aff}(B_l) \otimes \text{Aff}(B_m)$ and $\text{Aff}(B_k) \otimes \text{Aff}(B_l) \otimes \text{Aff}(B_m) \rightarrow \text{Aff}(B_m) \otimes \text{Aff}(B_l) \otimes \text{Aff}(B_k)$ for any $k, l, m \in \mathbb{Z}_{\geq 1}$. Note that these relations include the equality of the powers of ζ for each tensor component. For example, the inversion relation tells

$$H(\alpha \otimes \beta) = H(\tilde{\beta} \otimes \tilde{\alpha}). \tag{D.6}$$

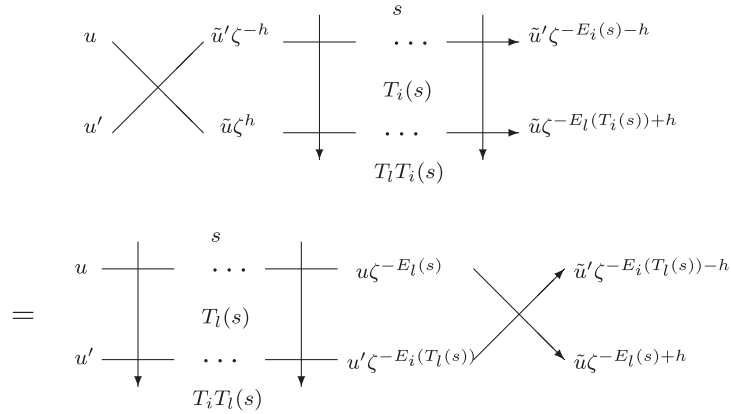
Now we consider BBS. An element $\alpha \in B_l$ can be interpreted as a capacity l carrier containing α_1 balls. When $l = 1$, it may also be regarded as a local BBS state containing $\alpha_1 (= 0, 1)$ ball. The BBS on the length L periodic lattice is a dynamical system on $B_1^{\otimes L}$. In what follows, a BBS state $s = (s_1, \dots, s_L) \in \{0, 1\}^L$ is identified with $(1 - s_1, s_1) \otimes \dots \otimes (1 - s_L, s_L) \in B_1^{\otimes L}$, which will also be denoted by $s_1 \otimes \dots \otimes s_L$.

The time evolution $s' = T_l(s)$ and the associated l th energy $E_l(s)$ are defined by the composition of the combinatorial R as follows:

$$\begin{array}{ccccccc}
 & s_1 & s_2 & & & s_L & \\
 u\zeta^0 & \downarrow & \downarrow & \dots\dots\dots & \downarrow & & u\zeta^{-E_l(s)} \\
 & s'_1 & s'_2 & & & s'_L &
 \end{array}$$

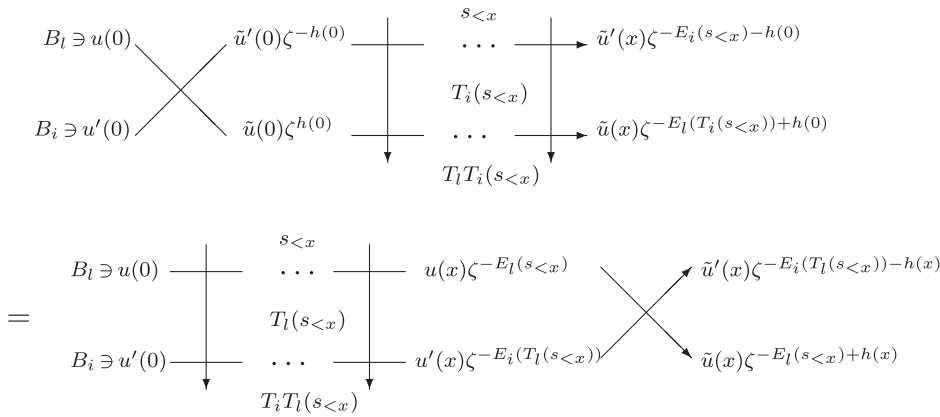
Here the carrier $u \in B_l$ is determined uniquely from $s = s_1 \otimes \dots \otimes s_L$ by the periodic boundary condition, namely, by requiring that it comes back to u itself after penetrating s provided that the ball density is not exactly $1/2$.

Let $u' \in B_l$ be another carrier for the time evolution $T_l(s) \rightarrow T_l T_l(s)$. Set $R : u'\zeta^0 \otimes u\zeta^0 \mapsto \tilde{u}\zeta^h \otimes \tilde{u}'\zeta^{-h}$ where $h = H(u' \otimes u)$. From the Yang–Baxter relation we have



Comparing the two sides we get the commutativity $T_l T_i(s) = T_i T_l(s)$ and the energy conservation $E_i(s) = E_i(T_l(s)), E_l(s) = E_l(T_i(s))$ as is well known.

Now consider the intermediate stage where the carriers have only gone through the first $x - 1$ local states $s_{<x} = s_1 \otimes \dots \otimes s_{x-1}$. To systematize the notation we write u, u', h in the above diagram as $u(0), u'(0), h(0)$. Then the corresponding diagram looks as



where $h(x) = H(u'(x) \otimes u(x))$. The carriers $u(x)$ and $u'(x)$ (resp. $\tilde{u}(x)$ and $\tilde{u}'(x)$) at this position do not yet have to return to the initial ones $u(0)$ and $u'(0)$ (resp. $\tilde{u}(0)$ and $\tilde{u}'(0)$). Define the local observables

$$\hat{\eta}_i^{(l)}(x) = H(u'(x) \otimes u(x)), \quad \hat{\eta}_l^{(i)}(x) = H(\tilde{u}(x) \otimes \tilde{u}'(x)). \tag{D.7}$$

Then the following properties are satisfied.

$$(i) \quad \hat{\eta}_i^{(l)}(x) = \hat{\eta}_l^{(i)}(x), \tag{D.8}$$

$$(ii) \quad \begin{cases} E_l(T_i(s_{<x})) - E_l(s_{<x}) + \hat{\eta}_l^{(i)}(x) - \hat{\eta}_l^{(i)}(0) = 0, \\ E_i(T_l(s_{<x})) - E_i(s_{<x}) + \hat{\eta}_i^{(l)}(x) - \hat{\eta}_i^{(l)}(0) = 0. \end{cases} \tag{D.9}$$

In fact (i) is a consequence of (D.6). As for (ii) both relations follow simultaneously by comparing the powers of ζ in the above diagram using (i). The upper relation, for instance, is nothing

but the space $[0, x]$ -integrated equation of continuity for E_l with respect to the time evolution T_i , where $\hat{\eta}_i^{(i)}(x)$ plays the role of local current at x .

As an example, $\hat{\eta}_2^{(3)}(x)$ associated with T_2T_3 are given in red letters in the top panel of figure 3. On the other hand, $\hat{\eta}_3^{(2)}(x)$ associated with T_3T_2 are given similarly in the bottom panel of figure 3. One can observe the equality $\hat{\eta}_2^{(3)}(x) = \hat{\eta}_3^{(2)}(x)$ everywhere. In this example, $\hat{\eta}_3^{(2)}(x) = \hat{\eta}_\infty^{(2)}(x)$ holds and it coincides with the carriers for T_2 , which is indeed the ball current.

ORCID iDs

Atsuo Kuniba  <https://orcid.org/0000-0002-1472-1138>

Grégoire Misguich  <https://orcid.org/0000-0002-7012-3204>

Vincent Pasquier  <https://orcid.org/0000-0002-0471-5199>

References

- [1] Takahashi D and Satsuma J 1990 A soliton cellular automaton *J. Phys. Soc. Japan* **59** 3514–9
- [2] Inoue R, Kuniba A and Takagi T 2012 Integrable structure of box–ball systems: crystal, Bethe ansatz, ultradiscretization and tropical geometry *J. Phys. A: Math. Theor.* **45** 073001
- [3] Levine L, Lyu H and Pike J 2020 Double jump phase transition in a soliton cellular automaton (arXiv:1706.05621)
- [4] Croydon D A, Kato T, Sasada M and Tsujimoto S 2018 Dynamics of the box–ball system with random initial conditions via Pitman’s transformation (arXiv:1806.02147)
- [5] Kuniba A, Lyu H and Okado M 2018 Randomized box–ball systems, limit shape of rigged configurations and thermodynamic Bethe ansatz *Nucl. Phys. B* **937** 40–271
- [6] Ferrari P A and Gabrielli D 2020 BBS invariant measures with independent soliton components *Electron. J. Probab.* **25** 1–26
- [7] Ferrari P A, Nguyen C, Rolla L T and Wang M 2020 Soliton decomposition of the box–ball system (arXiv:1806.02798)
- [8] Lewis J, Lyu H, Pylyavskyy P and Sen A 2020 Scaling limit of soliton lengths in a multicolor box–ball system (arXiv:1911.04458)
- [9] Croydon D A and Sasada M 2019 Invariant measures for the box–ball system based on stationary Markov chains and periodic Gibbs measures *J. Math. Phys.* **60** 083301
- [10] Croydon D A and Sasada M 2021 Generalized hydrodynamic limit for the box–ball system *Commun. Math. Phys.* **383** 427–63
- [11] Kuniba A and Lyu H 2020 Large deviations and one-sided scaling limit of randomized multicolor box–ball system *J. Stat. Phys.* **178** 38–74
- [12] Kuniba A, Misguich G and Pasquier V 2020 Generalized hydrodynamics in box–ball system *J. Phys. A: Math. Theor.* **53** 404001
- [13] Castro-Alvaredo O A, Doyon B and Yoshimura T 2016 Emergent hydrodynamics in integrable quantum systems out of equilibrium *Phys. Rev. X* **6** 041065
- [14] Bertini B, Collura M, De Nardis J and Fagotti M 2016 Transport in out-of-equilibrium XXZ chains: exact profiles of charges and currents *Phys. Rev. Lett.* **117** 207201
- [15] Doyon B 2020 Lecture notes on generalised hydrodynamics *SciPost Phys. Lect.* **018**
- [16] Rigol M, Dunjko V, Yurovsky V and Olshanii M 2007 Relaxation in a completely integrable many-body quantum system: an *ab initio* study of the dynamics of the highly excited states of 1D lattice hard-core bosons *Phys. Rev. Lett.* **98** 050405
- [17] Doyon B and Spohn H 2017 Dynamics of hard rods with initial domain wall state *J. Stat. Mech.* **073210**
- [18] Doyon B, Yoshimura T and Caux J S 2018 Soliton gases and generalized hydrodynamics *Phys. Rev. Lett.* **120** 045301
- [19] Doyon B 2019 Generalized hydrodynamics of the classical Toda system *J. Math. Phys.* **60** 073302
- [20] Bastianello A, Doyon B, Watts G and Yoshimura T 2018 Generalized hydrodynamics of classical integrable field theory: the sinh-Gordon model *SciPost Phys.* **4** 045

- [21] Kuniba A, Misguich G and Pasquier V 2021 Generalized hydrodynamics in complete box–ball system for $U_q(\widehat{sl}_n)$ *SciPost Phys.* **10** 095
- [22] Touchette H 2009 The large deviation approach to statistical mechanics *Phys. Rep.* **478** 1–69
- [23] Yang C N and Yang C P 1969 Thermodynamics of a one-dimensional system of bosons with repulsive delta-function interaction *J. Math. Phys.* **10** 1115–22
- [24] Zakharov V E 1971 Kinetic equation for solitons *JETP* **33** 538
- [25] El G A 2003 The thermodynamic limit of the Whitham equations *Phys. Lett. A* **311** 374–83
- [26] El G A and Kamchatnov A M 2005 Kinetic equation for a dense soliton gas *Phys. Rev. Lett.* **95** 204101
- [27] Ferrari P A, Nguyen C, Rolla L T and Wang M 2021 Soliton decomposition of the box–ball system (arXiv:1806.02798)
- [28] Myers J, Bhaseen J, Harris R J and Doyon B 2020 Transport fluctuations in integrable models out of equilibrium *SciPost Phys.* **8** 007
- [29] Doyon B and Myers J 2020 Fluctuations in ballistic transport from Euler hydrodynamics *Ann. Henri Poincaré* **21** 255–302
- [30] Mendl C B and Spohn H 2015 Current fluctuations for anharmonic chains in thermal equilibrium *J. Stat. Mech.* P03007
- [31] Ilievski E and De Nardis J 2017 Microscopic origin of ideal conductivity in integrable quantum models *Phys. Rev. Lett.* **119** 020602
- [32] Ilievski E and De Nardis J 2017 Ballistic transport in the one-dimensional Hubbard model: the hydrodynamic approach *Phys. Rev. B* **96** 081118
- [33] Doyon B and Spohn H 2017 Drude weight for the Lieb–Liniger Bose gas *SciPost Phys.* **3** 039
- [34] Bulchandani V B, Vasseur R, Karrasch C and Moore J E 2018 Bethe–Boltzmann hydrodynamics and spin transport in the XXZ chain *Phys. Rev. B* **97** 045407
- [35] Krajnik Z, Ilievski E, Prosen T and Pasquier V 2021 Anisotropic Landau–Lifshitz model in discrete space-time *SciPost Phys.* **11** 051
- [36] De Nardis J, Doyon B, Medenjak M and Panfil M 2022 Correlation functions and transport coefficients in generalised hydrodynamics *J. Stat. Mech.* 014002
- [37] Spohn H 2018 Interacting and noninteracting integrable systems *J. Math. Phys.* **59** 091402
- [38] Krajnik Z, Schmidt J, Pasquier V, Ilievski E and Prosen T 2022 Exact anomalous current fluctuations in a deterministic interacting model *Phys. Rev. Lett.* **128** 160601
- [39] Krajnik Z, Ilievski E and Prosen T 2022 Absence of normal fluctuations in an integrable magnet *Phys. Rev. Lett.* **128** 090604